SANDIA REPORT

SAND95–0196 • UC–704
Unlimited Release
Printed February 1995

Progress Report: High Temperature Solder Alloys for Underhood Applications

C. A. Drewien, F. G. Yost, S. Sackinger,
J. Kern, M. W. Weiser

Prepared by
Sandia National Laboratories
Albuquerque, New Mexico 87185 and Livermore, California 94550
for the United States Department of Energy
under Contract DE-AC04-94AL85000

Issued by Sandia National Laboratories, operated for the United States Department of Energy by Sandia Corporation.

Available to DOE and DOE contractors from
Office of Scientific and Technical Information
PO Box 62
Oak Ridge, TN 37831

Prices available from (615) 576-8401, FTS 626-8401

Available to the public from
National Technical Information Service
US Department of Commerce
5285 Port Royal Rd
Springfield, VA 22161

NTIS price codes
Printed copy: A03
Microfiche copy: A01

DISCLAIMER

Portions of this document may be illegible in electronic image products. Images are produced from the best available original document.

Distribution
Category UC-704

SAND95-0196
Unlimited Release
Printed February 1995

Progress Report: High Temperature Solder Alloys for Underhood Applications

C. A. Drewien, F. G. Yost, S. Sackinger,
Materials and Process Sciences Center,
Sandia National Laboratories
and
J. Kern and **M. W. Weiser** ,
Mechanical Engineering Department,
University of New Mexico

Abstract

Under a cooperative research and development agreement with General Motors Corporation, lead-free solder systems including the flux, metallization, and solder are being developed for high temperature, underhood applications. Six tin-rich solders, five silver-rich metallizations, and four fluxes were screened using an experimental matrix whereby every combination was used to make sessile drops via hot plate or Heller oven processing. The contact angle, sessile drop appearance, and in some instances the microstructure was evaluated to determine combinations that would yield contact angles of less than 30°, well-formed sessile drops, and fine, uniform microstructures. Four solders, one metallization, and one flux were selected and will be used for further aging and mechanical property studies.

INTRODUCTION

As technology advances, electrical component size decreases, and the number of input/output terminations increases[1]. This change in technology has lead to an increase in the number of solder joints with small joint dimensions. The benefits of shrinking solder joint dimensions are numerous (e.g. increased speed, greater packaging density, and so forth), but the reliability of the small solder joints becomes an issue.

Reliability of a solder joint depends upon alloy mechanical strength, voids, leaching, creep, fatigue, and excessive intermetallic compound formation[2]. Many of these factors are temperature dependent, and a major concern for reliability is the effect of athermal or isothermal cycling upon solder microstructure and properties. In terms of reliability, any high temperature exposure may cause formation of a brittle intermetallic in the solder joint, which may fracture catastrophically under the tensile or shear stress of the joint. The failure (electrical open) of a single solder joint could render an entire electronic assembly inoperable[1]. Aging studies and elevated temperature properties are often investigated when evaluating reliability issues in solder technology.

While the lead-tin (Pb-Sn) solders have fulfilled the requirements for reliable solder joints, alternative solder systems are now being investigated because new environmental regulations are limiting the use of toxic lead worldwide[2]. Low melting point binary, ternary, and quaternary metallic systems such as Sn-Ag, Sn-Bi, Sn-In, Sn-Sb, Sn-Zn, Sn-Ag-Sb, Sn-Ag-Cu, Sn-Ag-In, Sn-Ag-Sb, Sn-Ag-Zn, Sn-Bi-Sb, Sn-Bi-Zn, Sn-Ag-Bi-Cu, Sn-Ag-Bi-In, and Sn-Ag-Bi-Sb are under consideration for lead-free solder alternatives, and some data on these potential solders are available in the literature[2, 7, 8-11]. Of these systems, the silver-tin (3.5Ag-96.5Sn) eutectic alloy has shown the most promising results as a lead-free alternative, offering better mechanical properties--higher creep resistance[3], higher strength and lower ductility[3], better low cycle fatigue resistance[4], and higher impact resistance[5]--and high temperature performance--up to 100 °C[6] due to its higher melting point--than the Pb-Sn system.

In this investigation, General Motors Corporation (AC Rochester) and Sandia National Laboratories are working together through a cooperative research and development agreement (CRADA) in order to develop high temperature materials and electronic systems for critical components that will be mounted to automotive engines. In particular, a lead-free solder system including the solder, flux, and substrate metallization for an alumina substrate is being sought for high temperature, underhood automotive applications. In an underhood automotive environment, solders need to function at higher than normal temperatures and possess greater mechanical reliability than in many other applications, and exhibit a microstructure that does not form excessive intermetallic layers or voids with aging. The higher melting point Sn-Ag based solders, newly developed and commercially available, are being considered for underhood automotive applications.

PURPOSE

The purpose of this study is to i.) investigate lead-free solder systems based upon Sn-Ag alloys for wetting behavior, aging properties, and mechanical integrity, ii.) recommend a substrate metallization, flux, and solder system(s) for high temperature, underhood applications based upon desired properties, and iii.) demonstrate production of solder joints for high temperature underhood applications using standard commercial processing parameters.

PROCEDURE

Materials Used

Six solders with melting points between 208 and 221 °C, four fluxes, and five metallizations were chosen as possible candidates for higher temperature, underhood applications. Six solder alloys were chosen based upon previous development and characterization work in which compositions, melting points, microstructure, and contact angle measurements [12] were investigated. The solders chosen as potential candidates for the required application are listed in Table IA along with compositions in weight percent (w/o) and known melting points determined using differential scanning calorimetry. Two solders with proprietary compositions containing tin-copper-silver (SCA) and tin-copper-silver-bismuth (SCAB) and four other solders--tin-silver-bismuth (SAB), tin-silver-bismuth-antimony (SABSb), Castin, and the tin-silver eutectic or Indalloy 121--were selected for use in this study.

The fluxes chosen as possible candidates are referred to herein as RMA, no clean, water soluble, and citric. The fluxes are Alpha products--Alpha 611 Resin-Mildly-Activated flux cut fifty percent with isopropanol, Alpha 250-hf Water Soluble flux, Citric-hf-1189, and No Clean 922-cx.

The Indalloy 121 wire was purchased from Indium Corporation of America. The Castin and the SAB solder wires were purchased from AIM (American Iron and Metal Company); the SCAB and the SCA solder wires were purchased from AMES Laboratory.

Silver-rich pastes containing various alloying elements were chosen for metallization pads for the solders. The metallized inks, used to screen print alumina substrates, were manufactured by E. I. DuPont de Nemours and Company. Manufacturer reported compositions of solids in the ink are listed in Table IB. Metallizations are referred to herein by their numerical designation-5081/5082, 6160, 6175, 6277, 7484. Note that the 5081/5082 is two metallizations--one on top of the other. The metallizations were fired in a furnace to a peak temperature of 850 °C for 10 minutes and cooled.

Sample Preparation

Solder and Flux Preparation--In order to determine the best combinations of solder, flux, and metallization, an experimental matrix was designed that would allow for every combination of solder, flux and metallization to be tested and evaluated for contact angle and appearance. The solder alloys in wire form were cut into 10 or 20 mg segments, placed in a pitre dish with RMA flux, and heated in air to 260 °C. Once the flux started to boil, the solder particles melted and formed balls. The dish was removed from the heat and isopropanol was added to facilitate removal of the solder ball. Each solder ball was accurately weighed using a Mettler balance.

Table IA--Solders Used in Study

SOLDER ALLOY	COMPOSITION (w/o)	MELTING POINT (°C) (onset at 10 °C/min)
Sn-Cu-Ag (SCA)	93.6 Sn, 1.76 Cu, 4.64 Ag (proprietary)	217
Sn-Cu-Ag-Bi (SCAB)	88.9 Sn, 1.6 Cu, 4.5 Ag, 5.0 Bi (proprietary)	~208
Sn-Ag-Bi (SAB)	91.9 Sn, 3.33 Ag, 4.8 Bi	211.99*
Sn-Ag-Bi-Sb (SABSb)	92 Sn, 1 Ag, 4 Bi, 3 Sb	217.22
Castin	96.2 Sn, 2.5 Ag, 0.8 Cu, 0.5 Sb	216
IND 121	96.5 Sn, 3.5 Ag	221

*Onset at 1 °C/min.

Table IB--Metallizations Used in Study

METALLIZATION SUBSTRATE	REPORTED SOLIDS IN INK (w/o)
5081	75 Ag, 7 Pt
5082	79 Ag, 6 Pt
6160	83 Ag
6175	60 Ag, 12 Pd
6277	62 Ag, 10 Pd, 1 Ru
7484	50 Ag, 17 Pd, 1 Ru

Heat Treatment

Hot Plate--A metallization substrate, covered with flux, was placed upon a hot plate heated to 260 °C. After four minutes, a 10 ± 1 mg solder ball, formed from wire, was placed on the heated substrate and heated for 2 minutes after becoming molten. The sample was then removed from the heat and air cooled. The entire heat treatment was recorded using a video camera. A matrix of 120 combinations in which each of the six solders, five metallizations, and four fluxes was used to prepare samples.

Heller Oven--A 20 ± 1 mg solder ball saturated in flux was placed on the metallization. Additional flux was added to create a puddle of flux around the solder ball. This system was then placed into a Heller Reflow Oven model 988C, used to produce samples according to a standard industrial heat treatment process. Temperature profiles for each of the solder alloys were created according to melting point information; the information was programmed into the control of the Heller Reflow oven. Confirmation of the temperature profile was achieved by soldering a thermocouple to a metallized substrate and monitoring the temperature during the profile. The average length of a profile was seven minutes, the average peak temperature was 240 °C, and the belt speed was 27 cm per second. An example of a typical temperature profile is shown in Figure 1. These profiles were tailored after manufacturer's recommendations.

After the initial down selection of the 120 samples, a matrix of 24 samples was designed. These samples were also reflowed through the Heller oven to simulate

industrial processes; thus, a total of 48 samples were formed. This matrix consisted of four solder alloys, three metallizations, and two fluxes.

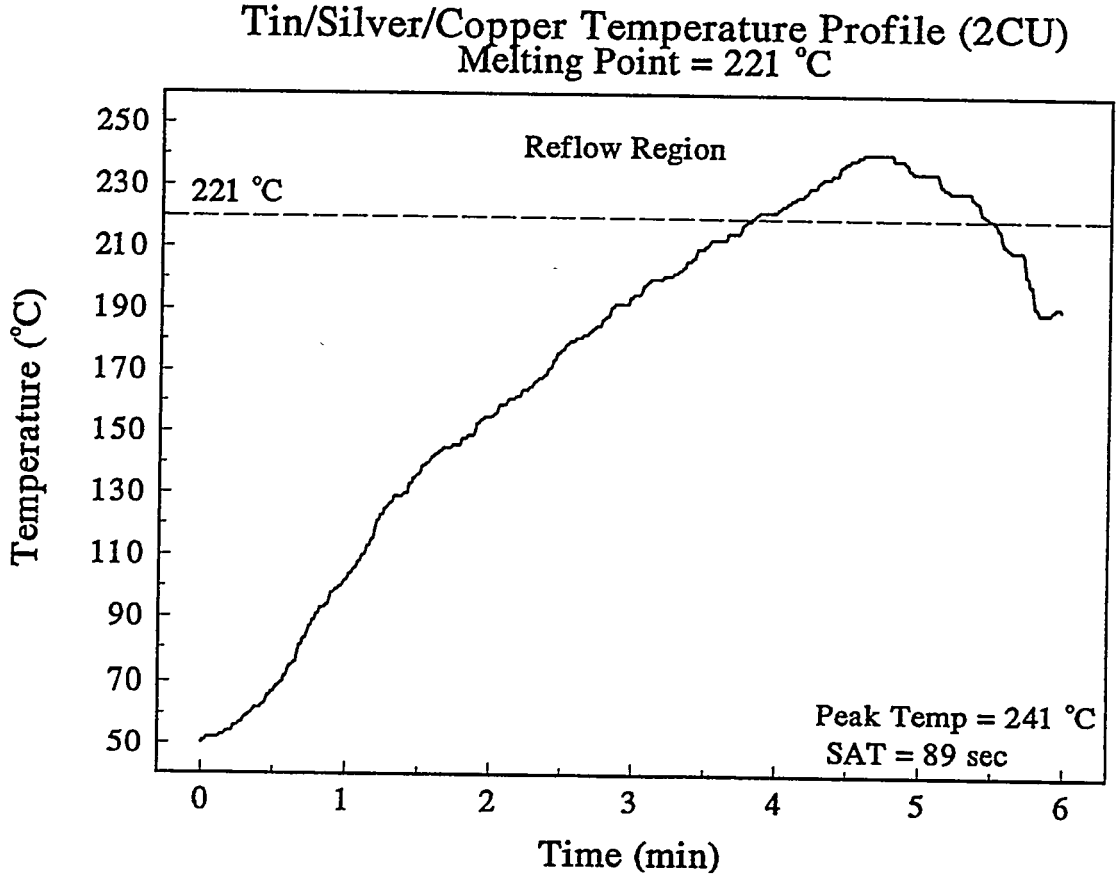

Figure 1--Temperature profile for Tin-Copper-Silver solder alloy.

Contact Angle Measurement

After reflow, the samples were cleaned with trichloroethylene (TCE) to remove the flux residue on the metallization and the sessile drop. TCE was placed in a large beaker and heated to 87°C; at this temperature vapors can be seen rising along the sides of the beaker. Samples were placed in the TCE vapors for two minutes. After this time, the sample and was agitated in a solution of isopropyl alcohol for another two minutes. The sample was dried with argon gas. This cleaning process removed the flux from the sessile drops. However, the flux adhered to the metallization's surface, causing discoloration; this did not interfere with measuring the contact angles.

The contact angles of the sessile drops on the metallization were obtained with a system called "Image Pro-Plus", a software[13] package for micro-imaging. This software is capable of measuring angles to an accuracy of 92±3 percent. Figure 2 shows a schematic setup for measuring the contact angles. This system allows a user to freeze an image of a sample and measure two contact angles per picture frame.

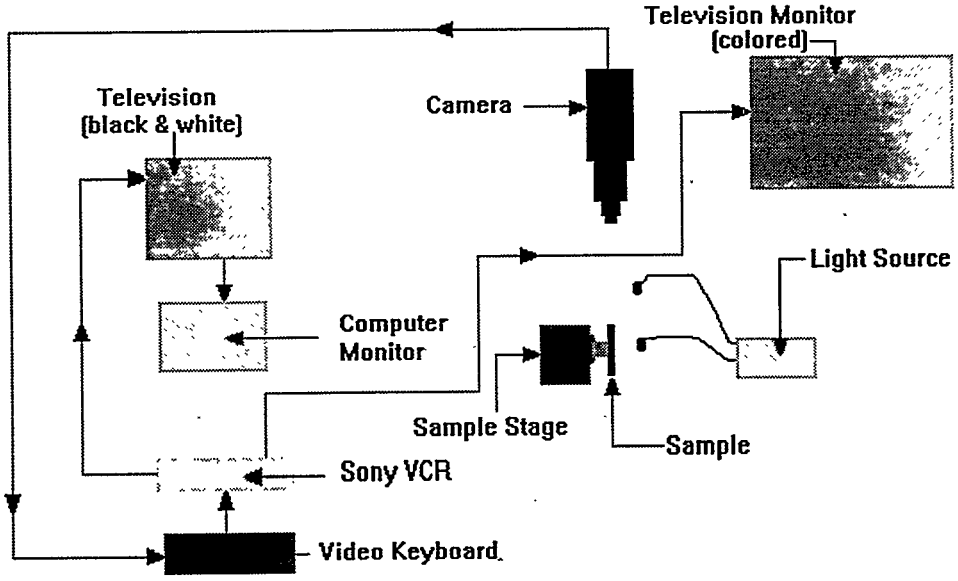

Figure 2--Schematic setup for obtaining contact angles from a sample.

A total of four images were obtained by rotating the sample 45° increments, giving a total of eight contact angles measurements per alloy/flux/metallization combination. In order to obtain measurement of the contact angles, a baseline was established for the solder/metallization interface. The beginning point of this baseline became the vertex of the angle from which another line was positioned along the slope of the sessile drop to form an angle. Figure 3 shows an approximate image by which two contact angles were measured per rotation.

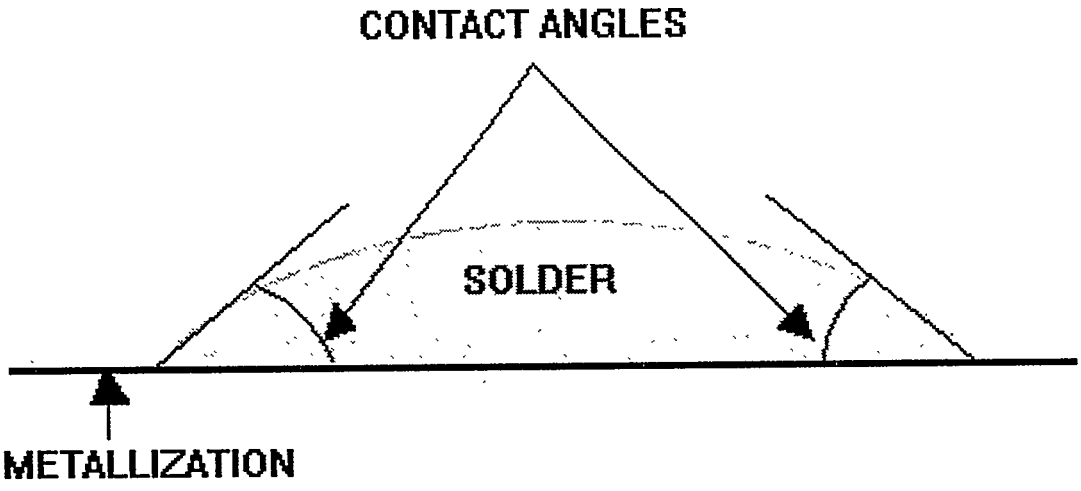

Figure 3--Measuring of two contact angles at solder/metallization joint.

Appearance

The appearances of the sessile drops were qualitatively rated on a scale of 1 through 5 based upon the ranking criterion shown in Table II. Figure 4 shows the appearance of the drops with appearance values of 1 through 5.

Table II--A list of the descriptive appearances of the sessile drops after wetting, and the assigned values.

VALUES	APPEARANCE
1	smooth, well formed droplet
2	relatively smooth droplet with some footing
3	fried egg
4	badly fried egg; center is cratered
5	badly dewetted
6	did not wet

Selection of Preferred Solder, Flux, Metallization Combinations

In order to select solder systems with preferred contact angles and appearances, the data for contact angle and appearance were compiled, and the product of the angle and appearance was computed. A low value of contact angle is desirable for good wetting behavior, and a low value of appearance indicates that a well developed sessile drop had formed. Therefore, a low product of contact angle and appearance was sought. The effect of atmosphere on the contact angle, appearance, and product was investigated for the 24 trials heat treated on both the hot plate and in the Heller oven. This was done by substracting the value for a given trial on the hot plate from that done in the Heller oven. This data was analyzed statistically to determine which combinations of solder, metallization, and flux were most affected by the change of atmosphere.

Microstructural Analysis

Metallization pads and/or solder on metallization pads were sectioned along a laser scribe in the alumina. The sample was then cold mounted in alumina filled epoxy for cross-sectional analysis. Mounted specimens were polished on a fixed diamond wheel and then polished on 6 μm and 1 μm diamond paste using Buehler's Metadi extender and a nylon cloth. Final polishing was performed on Stuer's OPS suspension--colloidal silica at a pH of 7.5--on microcloth.

Cross-sectional images and topograph images of the metallization and the metallization/solder combination were obtained on a JEOL 6400 scanning electron microscope (SEM) operated at an accelerating voltage of 20 kV. Secondary and back-scattered electron images were obtained on the polished surfaces.

Compositional Analysis

Metallization compositions were determined using a JEOL 8600 Superprobe electron microprobe analyzer operated at 15 kV. Samples were carbon coated, and elemental distribution photomicrographs were obtained for all elements detected in the metallization and alumina substrate using wavelength dispersive detectors. Quantitative compositional analyses of the outer regions of the metallization were determined using wave-length dispersive measurements; 10 random spots along the outer edge of the

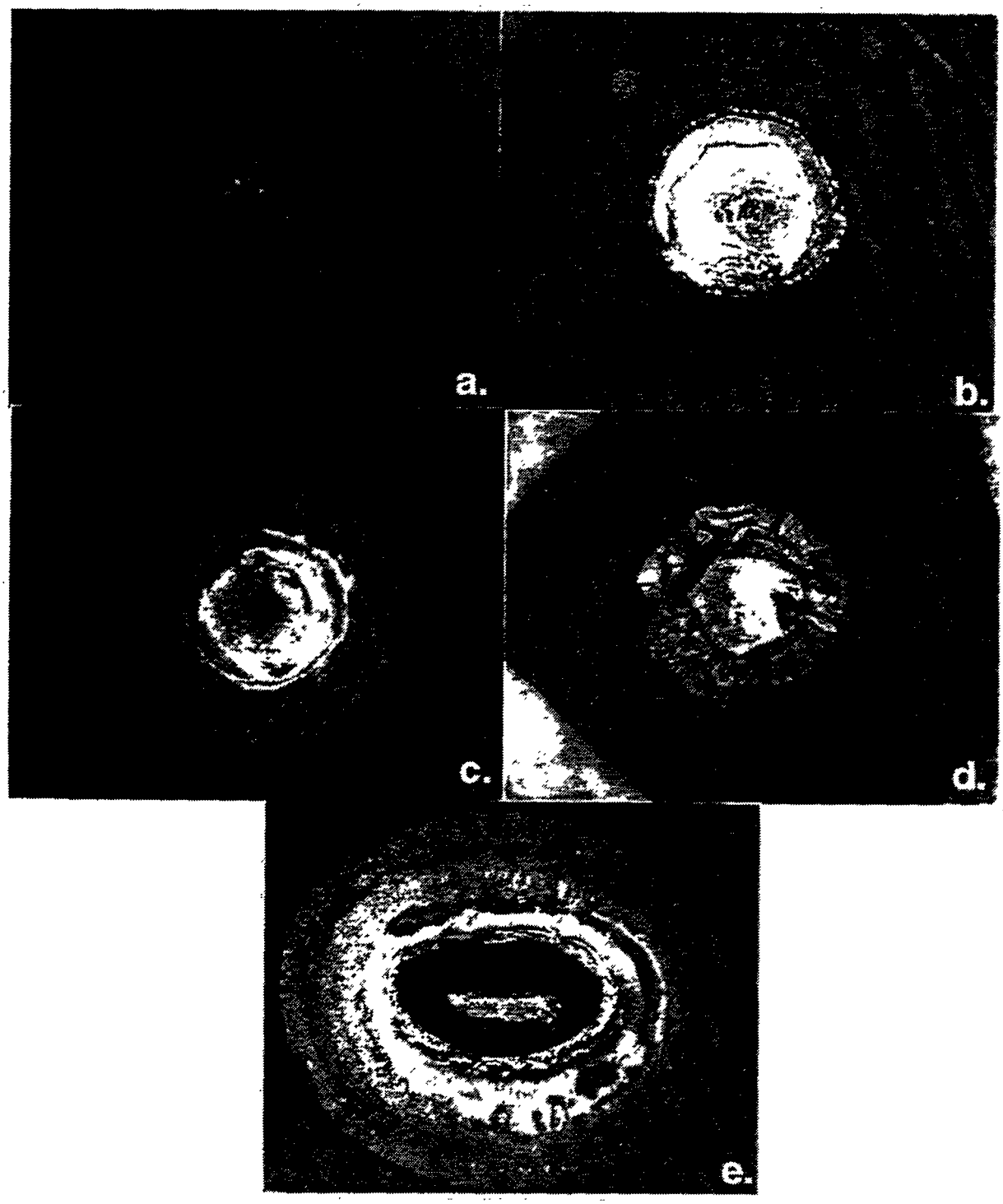

Figure 4--Sessile Drop Appearances (9x)

a.) Value 1--Smooth, well-formed

b.) Value 2--Smooth with footing

c.) Value 3--Fried Egg

d.) Value 4--Badly fried egg, center is cratered

e.) Value 5--Dewetted

metallization were analyzed. The x-ray lines used for each element in the analyses are listed in Table III where data are reported as the average value of composition from the ten data points along with error bars for 95% confidence level in the analyses. Counting error statistics and other systematic errors were not considered. A phi rho z correction was incorporated to correct the k value for matrix effects, however the influence of porosity was not taken into consideration.

Table III--X-ray Lines Used for Quantitative Composition Analysis

Element	Ag	Al	Bi	Ca	Co	Cu	Mg	Ni	Pb	Pd	Pt	Ru	Si
Line	Lβ	Kα	Mα	Kα	Kα	Kα	Kα	Kα	Mα	Lα	Mα	Lα	Kα

Finally, qualitative compositions of particles, inclusions, and phases other than the matrix phase observed in surface images of the metallization were determined using a Noran 5500 energy dispersive spectrometer (EDS) attached to the JEOL SEM.

RESULTS

Analysis of the Initial Wetting Experiment

The full factorial experiment was performed to investigate the wetting behavior of all six alloys on each of the five metallizations under the influence of all four fluxes in an air atmosphere. This resulted in a total of 120 different trials for this experiment. Eight contact angles were measured at approximately 45° angles around the perimeter of the sessile drop for all of the combinations except for three of the Indalloy 121 samples where only four (two cases) or five (one case) measurements could be made accurately. These contact angles were multiplied by the appearance to calculate a product that would be minimized for "good" wetting because both a small contact angle and a good appearance (low value) are desired.

The mean contact angle for each of the 15 main factors are plotted versus these factors in Figure 5. The overall mean contact angle is 25.13° which is below the value of 30°, an acceptable value for electronic solders. Only the mean contact angle for the 6175 metallization is greater than this value. There is a large amount of variation as is expected in such a comprehensive full factorial experiment where all combinations of the factors are examined. The Indalloy 121 solder alloy, 7484 metallization, and the RMA flux yielded the smallest mean contact angles. However, the extensive overlap of the error bars shows that merely selecting one or all of these factors will not result in the smallest contact angle.

The appearance of the sessile drop is a simple way to quickly determine if there are adverse reactions between the solder alloy and the metallization. The mean appearance of the sessile drop is plotted versus the main factors in Figure 6, which shows that the metallization has a strong effect on the appearance while the solder alloy and flux do not. The Ag (6160) and Ag/Pt (5081/5082) based metallizations have much better appearances than the other three metallizations, which are all Ag/Pd based.

Successful use of a solder/metallization/flux system requires that both the contact angle and the appearance be suitable. The product of these two responses is plotted in Figure 7 versus the main factors. Examination of this response for the metallizations shows that the 6160 and 5081/5082 metallizations have the most desirable values, resulting mainly from their very good appearances. The two Ag/Pd based metallizations that contain Ru have a reasonably good product as a consequence of their having the lowest mean contact angles, while the 6175 metallization has a very poor product.

The previous three figures showed some of the general trends in the contact angle and appearance versus the main factors. However, the large error bars indicate that there

are either significant interactions between the factors or that there are large experimental errors. In order to compare the variations due to the factors and their interactions with the variation due to noise and experimental error, an Analysis of Variance (ANOVA) was performed. This was done for each of the three responses using the true error for the contact angle and the product. The pooled error composed of the three-way interaction (alloy x metallization x flux) was used for the appearance because only one datum point was taken for each trial. This is justified because the mean square for the three-way interaction is only 36% as large as the next smallest mean square.

The calculations are summarized in Table IV where Num is the number of different settings or combinations, DOF is the degrees of freedom, SS is the sum of the squares, MS is the mean square or SS/DOF, F is the Fisher F-Test Statistic or the MS/MS_{error}. The alloy, flux, and metallization are denoted by A, F, and M, respectively. This analysis found that all of the factors and interactions were significant, as illustrated in Table IV. The minimum level of significance listed is really a severe under estimate of the true level of significance in most cases. This is a result of 99.5% being the highest level of significance that was tabulated in Montgomery[14]. The lowest level of significance found was 95% for the effect of the flux on the appearance.

Table IV--Contact Angle ANOVA Table for the Initial 120 Trial Experiment

Source	Num	DOF	SS	MS	*F*	Minimum Significance
Alloy	6	5	12037	2407.40	49.97	0.995
Flux	4	3	6018	2005.97	41.63	0.995
Metallization	5	4	22440	5610.06	116.44	0.995
A x F	24	15	13295	886.36	18.40	0.995
F x M	20	12	11713	976.12	20.26	0.995
M x A	30	20	13420	670.98	13.93	0.995
A x F x M	120	60	24887	414.79	8.61	0.995
Grand Mean		1				
Total		948	143752			
Error		829	39942	48.18		

The high levels of significance made it particularly difficult to down select a subset of the 120 trials for further study; it was not possible to base the decisions on one or two significant factors or factor interactions. The down selection process was aided by examining the product in more detail and by including external information as it became available.

The variability of the mean product as a function of metallization and alloy is illustrated in Figure 8. The relatively high variability of the 5081/5082 and 6160 metallizations resulted from a few very high values that can probably be classified as outliers. The values for the 7484 metallization were also fairly low with a limited number of higher values (>100). This analysis would indicate that these three metallizations should be selected for further study. However, concurrent accelerated environmental chamber studies indicated that the 6160 metallization was very easily corroded under atmospheric conditions as a consequence of its only significant metal constituent being silver. It was desired to keep three of the metallizations in the next experiment if possible; therefore, the 6277 metallization was selected as a third

metallization instead of 6160, because it had several alloy/flux combinations with low products.

Down selection of the fluxes was accomplished based upon a combination of analyzing the mean product and visual inspection of the metallizations after cleaning. The mean product is plotted versus the flux in Figure 9 for the three remaining metallizations using the same symbols as in Figure 8 to delineate the solder alloys. It is readily seen that the no clean and RMA fluxes resulted in smaller, more desirable mean products. The citric acid was observed to severely discolor the metallization. Based upon this information, the RMA and no clean fluxes were chosen for further study. RMA is the standard flux in use today, and industry desires to use a no clean flux.

Down selection of the solder alloys was more difficult to base upon the experimental results. Examination of Figure 9 for the no clean and RMA fluxes showed that the product is quite large for the Castin solder alloy on two of the three metallizations, so Castin was eliminated from further study. This same criterion could have been used to eliminate the tin-copper-silver (SCA) alloy, because the product is quite large for three of the six flux/metallization combinations. However, further testing will be performed on SCA before it is eliminated. The tin-silver-bismuth-antimony (SABSb) alloy was dropped from further consideration because of evidence that antinomy tends to make the solder joint brittle[15].

First Down Selection

Based upon the contact angles, appearances, and corrosion information, the following solder, flux, and metallizations were chosen for further analyses. This down selection process resulted in keeping the four solder alloys, three metallizations, and two fluxes listed in Table V.

Table V--Remaining Alloys, Metallizations, and Fluxes after Primary Down Selection

Solder Alloy	Metallization	Flux
Indalloy 121	5081/5082	No Clean
SAB	6277	RMA
SCA	7484	
SCAB		

Analysis of the Second Wetting Experiment

A full factorial experiment was performed to evaluate the wetting behavior of the remaining 24 combinations of alloy, metallization, and flux in an inert atmosphere (< 100 ppm oxygen) using the Heller oven. This permitted direct comparison of the results obtained in air with those obtained in the more industrially relevant processing through the Heller reflow oven. The responses for this experiment and the data from the same 24 combinations from the initial experiment are listed in Table VI. This data has been sorted in ascending order of the contact angle-appearance product for the Heller oven data since low values of this response are desired.

Table VI--Summary of Response for the Second Wetting Experiment

Alloy	Metalliz.	Flux	Heller Data			Hot Plate Data		
			Contact Angle	Appear	Product	Contact Angle	Appear	Product
SAB	7484	RMA	5.31	2.50	13.27	8.04	3.00	24.11
SCAB	5081/5082	RMA	15.03	1.50	22.54	21.55	1.17	23.86
SAB	5081/5082	NC	14.23	1.75	24.47	21.88	1.00	21.88
SAC	5081/5082	RMA	25.71	1.00	25.71	24.38	1.50	36.56
Ind 121	7484	NC	8.79	3.25	27.96	8.39	4.50	37.74
Ind 121	5081/5082	RMA	28.14	1.00	28.14	21.44	1.25	26.80
SAB	5081/5082	RMA	16.32	1.75	28.48	29.41	1.00	29.41
SCAB	6277	RMA	12.93	2.25	28.56	24.09	4.50	108.39
SCAB	7484	RMA	8.58	3.25	29.53	11.14	3.83	42.99
SAC	7484	RMA	9.46	3.25	29.84	7.75	4.50	34.88
Ind 121	5081/5082	NC	32.27	1.00	32.27	22.19	1.00	22.19
SAC	5081/5082	NC	32.36	1.00	32.36	30.00	1.00	30.00
SCAB	5081/5082	NC	21.66	1.50	32.48	21.79	1.00	21.79
SAC	6277	RMA	7.23	4.50	32.51	24.40	4.00	97.60
SAC	7484	NC	9.55	3.75	34.66	29.63	4.00	118.50
Ind 121	6277	RMA	8.09	4.50	36.39	7.19	4.83	34.65
SAB	7484	NC	10.13	4.25	43.22	20.66	2.50	51.66
SAB	6277	NC	13.62	3.25	43.81	21.30	1.50	31.95
SCAB	6277	NC	15.03	3.00	46.33	23.04	2.00	46.08
SAB	6277	RMA	11.83	4.00	47.30	4.91	2.50	12.28
Ind 121	6277	NC	11.94	4.00	47.78	8.00	4.50	36.00
SAC	6277	NC	15.48	3.50	54.16	26.70	4.00	106.80
SCAB	7484	NC	14.28	4.00	57.13	35.31	2.50	88.28
Ind 121	7484	RMA	12.53	5.00	62.63	6.24	4.83	30.24
		Mean	15.02	2.86	35.90	19.14	2.77	46.44
		Std. Dev.	7.78	1.31	13.61	8.99	1.49	31.64

Examination of Table VI shows that the mean contact angle and product are lower for the samples heat treated in the Heller reflow oven than those heat treated on the hot plate, while the mean appearance is slightly higher for the Heller oven samples. The significance of these differences was evaluated using the student T-test to see if the null hypothesis--that there is no difference--could be rejected. The differences are significant at the >97.5% level for the contact angle, >60% for the appearance, and >95% for the product. The difference could result from less oxide present on the Heller oven samples, allowing for further spreading of the sessile drop and further reaction with the metallization. The first of these is desirable, while the second is not.

The mean product from Table VI is plotted versus the metallization in Figure 10. The values for the 5081/5082 metallization were quite low and consistent. This is a consequence of the mean appearance of these samples ranging from 1 to 1.75 along with mean contact angle ranging from 14.23 to 32.36°. The mean product was higher and more variable for both the 6277 and 7484 metallizations. However, most of the variability is observed for the SAC and SCAB alloys. In addition, the appearance values for both of these metallizations were significantly higher than for the 5081/5082 metallization indicating that the alloy reacted more with the metallization. This is particularly evident for the Heller samples where the metallization accounted for 71.5% of the total observed variation in the appearance.

The significance of the factors and their interactions on each of the responses was analyzed via ANOVA for both methods of heat treatment. Elimination of some of the alloys, metallizations, and fluxes resulted in a large decrease in the level of significance for many of the factors and their interactions. The results of this analysis are summarized in Table VII. For heat treatment on the hot plate, the flux was very significant in determining the appearance while it had no significance for heat treatment in the Heller reflow oven. This indicated that a strong flux was important when soldering in air, while the flux had no measurable effect in an inert atmosphere. It is also seen that the alloy and the interaction between the flux and metallization had little or no effect on the product for heat treatment in the Heller reflow oven.

Final down selection for aging studies were based upon microstructural analyses, which are presented below.

Table VII--Factor and Interaction Significance in Second Wetting Experiment

Source	Num	DOF	Heller Data			Hot Plate Data		
			Appear	Contact Angle	Product	Appear	Contact Angle	Product
Alloy	4	3	0.950	0.995		0.750	0.995	0.995
Flux	2	1		0.995	0.995	0.975	0.995	0.995
Metalliz.	3	2	0.995*	0.995	0.995	0.900	0.995	0.995
A x F	8	3	0.975	0.995	0.995	0.750	0.900	0.995
F x M	6	2	0.750	0.950	0.750	0.900	0.995	0.995
M x A	12	6	0.995	0.995	0.995		0.995	0.995
A x F x M	24	6	0.995	0.995	0.995		0.995	0.995

*This factor accounted for 71.5% of the total variability and the real level of significance is far greater than this maximum tabulated value.

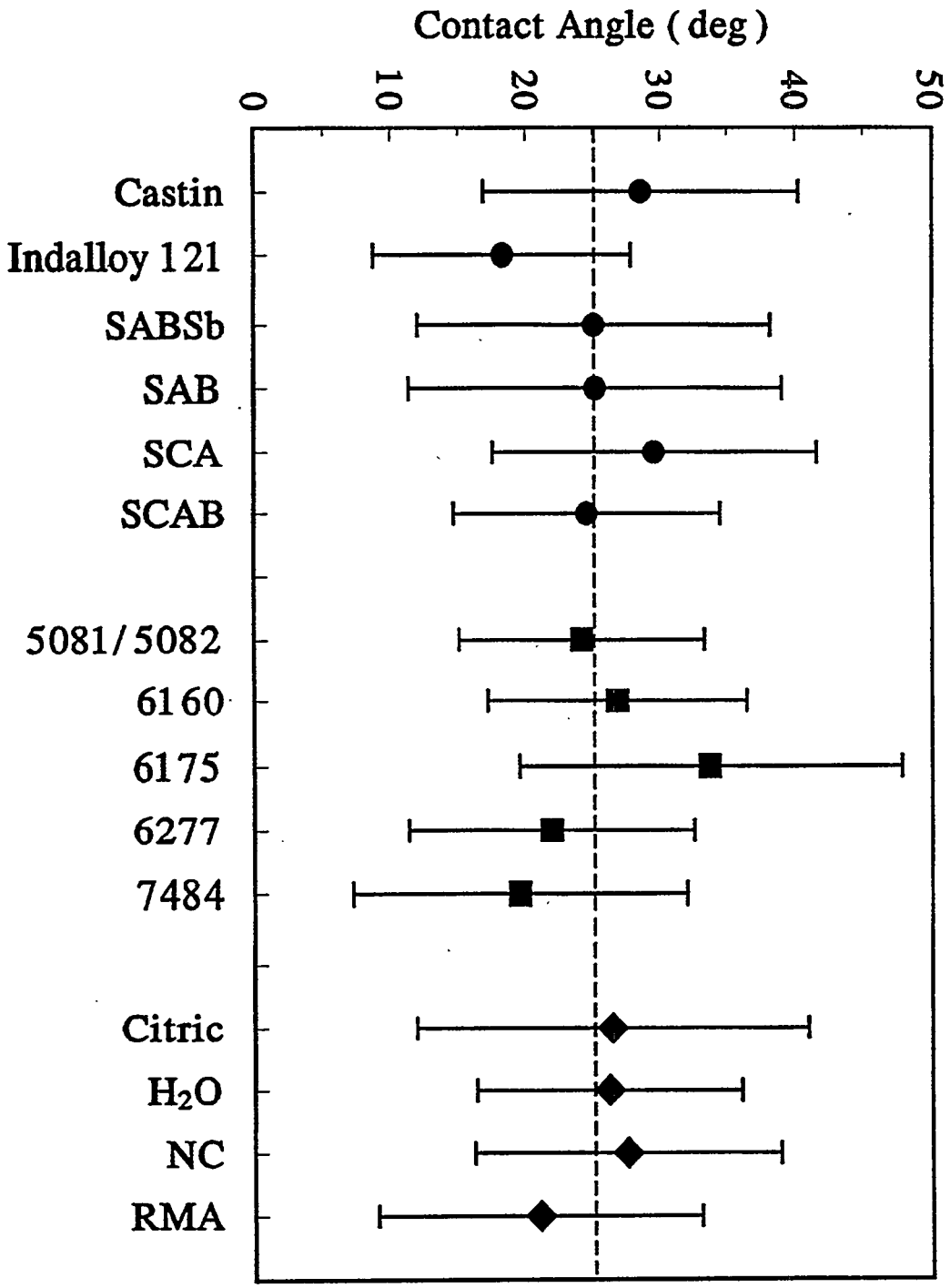

Figure 5

Mean contact angle with ±1 standard deviation error bars versus the main factors for the initial 120 trial experiment. The dashed line indicates the overall mean contact angle of 25.13°.

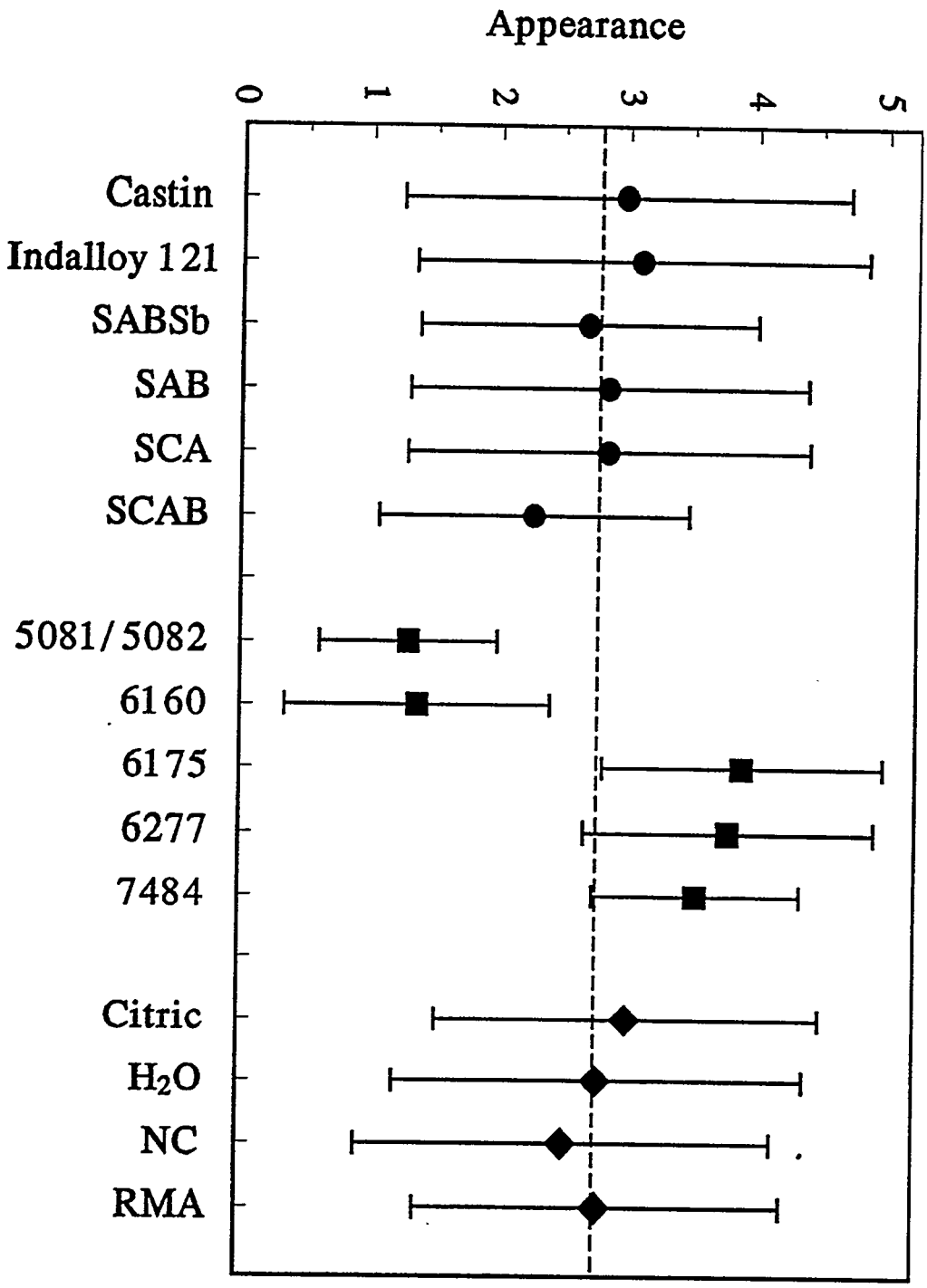

Figure 6

Mean appearance and ±1 standard deviation error bars versus the main factors for the initial 120 trial experiment. The dashed line indicates the overall mean appearance value of 2.79.

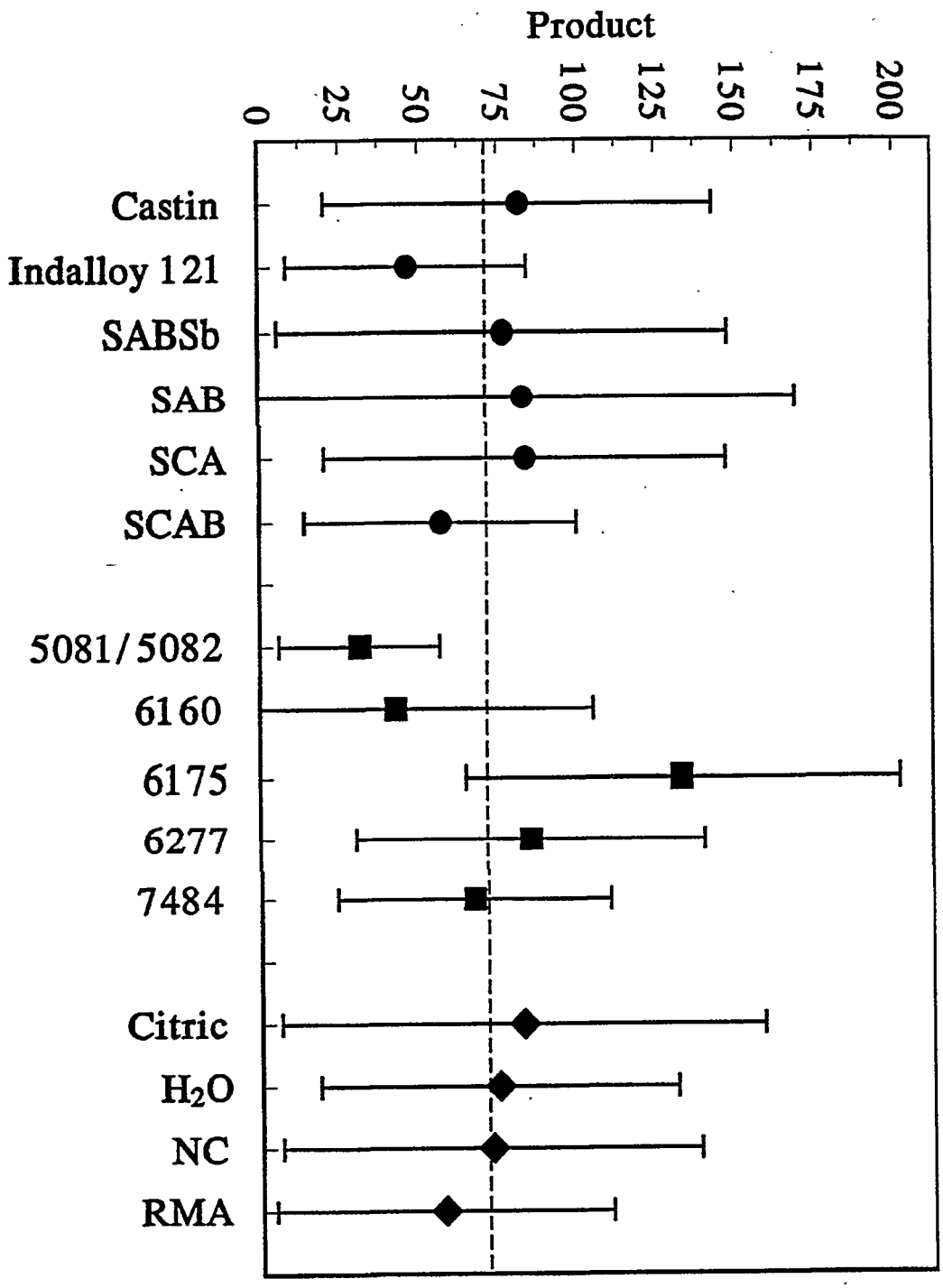

Figure 7

Mean product and ±1 standard deviation error bars versus the main factors for the initial 120 trial experiment. The dashed line indicates the overall mean appearance value of 71.4. The negative value of the lower end of the error bar for the 6160 metallization is a consequence of the distribution of products for this factor being extremely skewed since negative values are impossible.

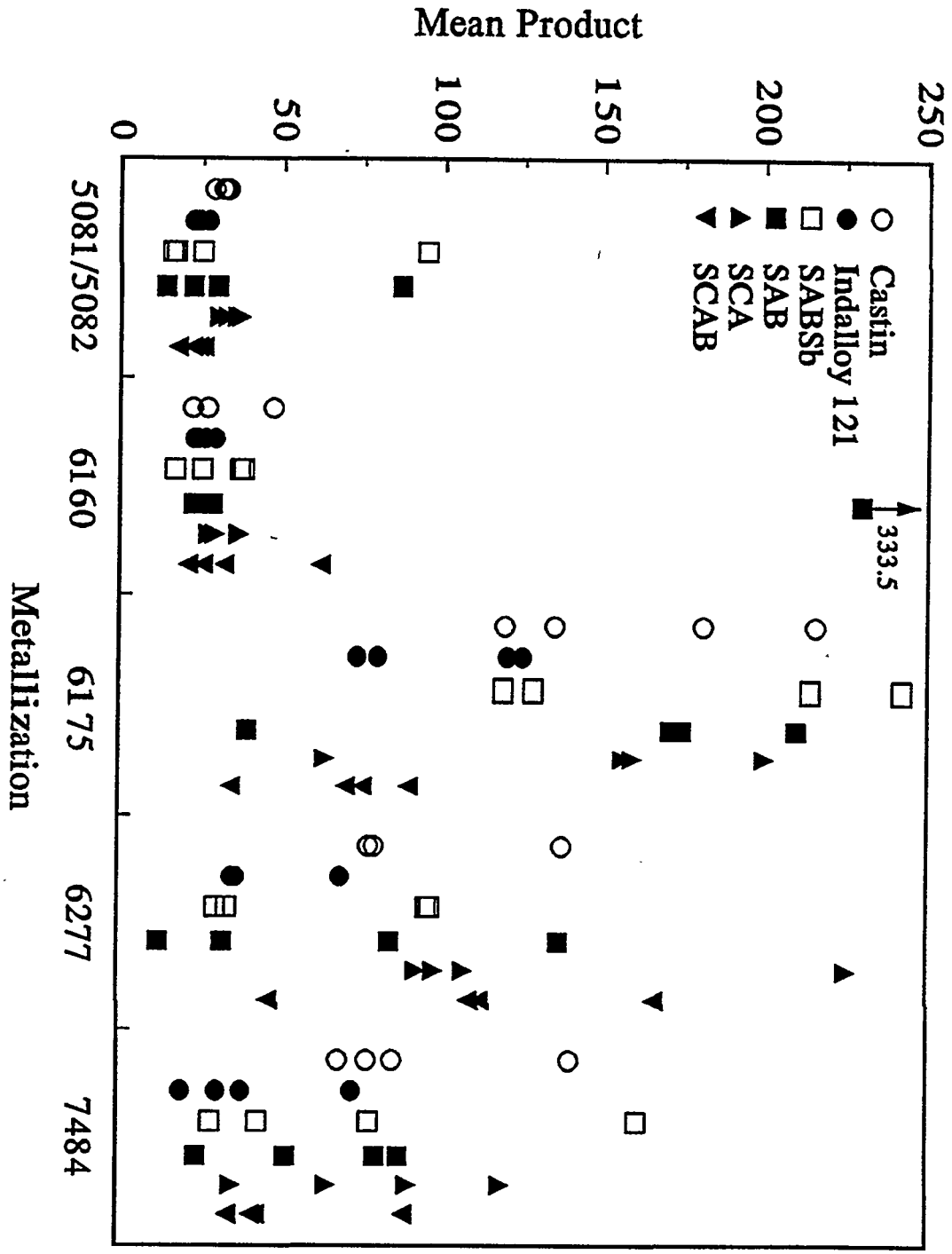

Figure 8

The mean product versus metallization for the initial wetting experiment with different symbol styles for the solder alloys. There are four markers for each combination of metallization and solder alloy corresponding to the four different fluxes.

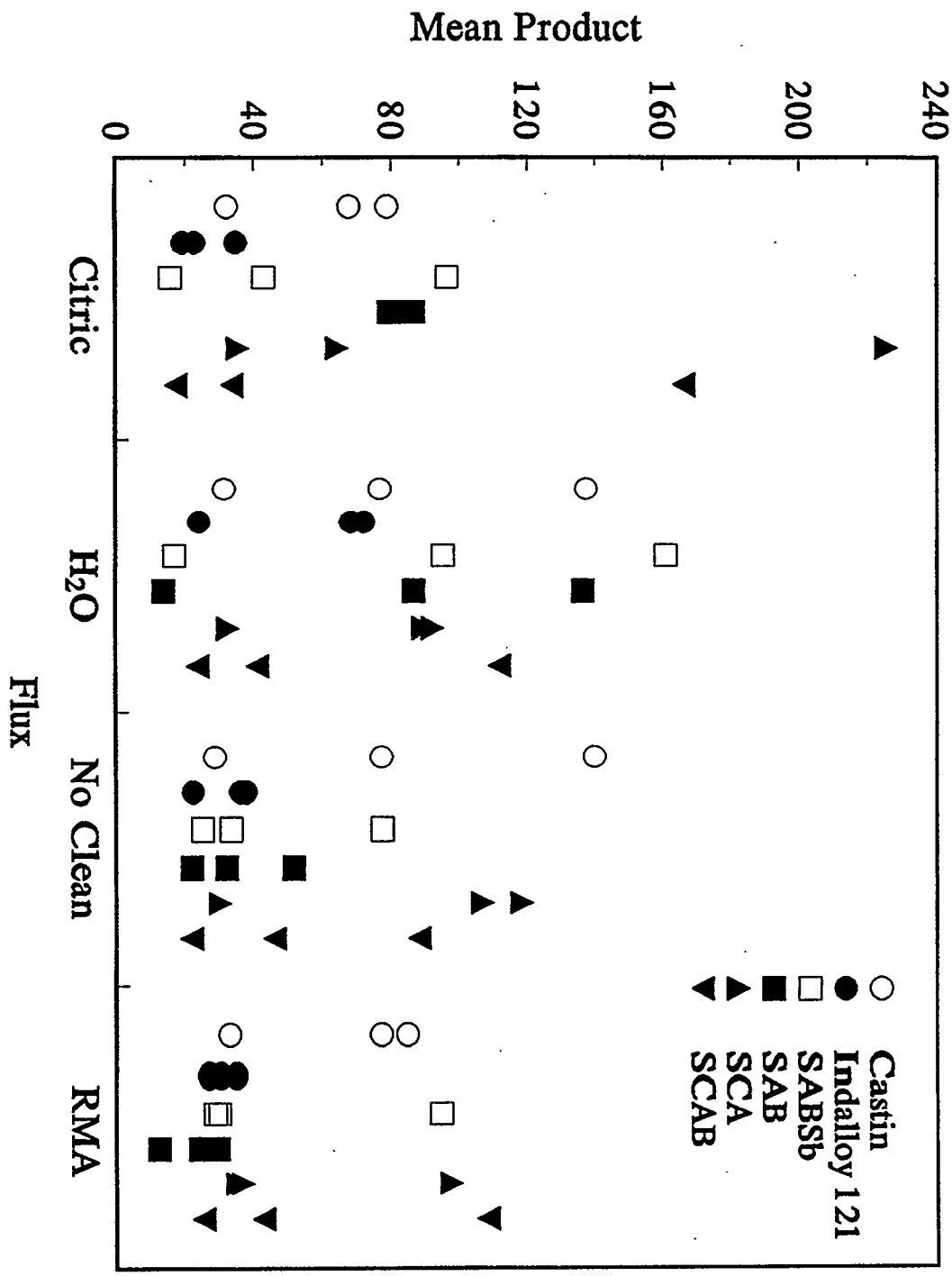

Figure 9

The mean product versus flux for three of the metallizations in the initial wetting experiment using different symbols for the solder alloys.

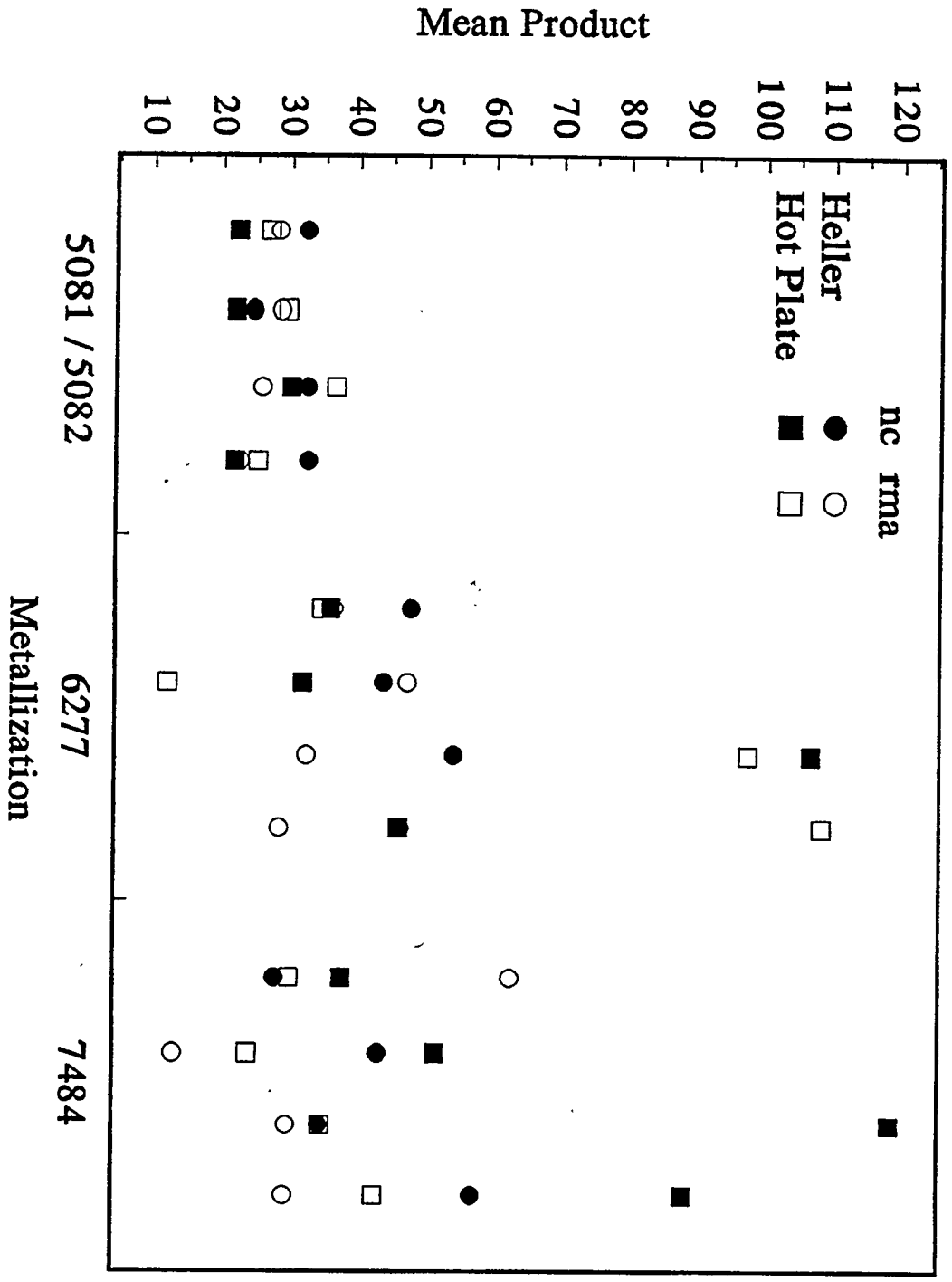

Figure 10

The mean product versus metallization for both the Heller oven and hot plate samples from the second wetting experiment. The solder alloys are in the same order for each metallization and are Indalloy 121, SAB, SAC, and SCAB from left to right.

Microstructural Analysis--Metallization Substrates

The compositions of the outermost region of the metallization were determined using wavelength dispersive spectroscopy in an electron microprobe. The average value of 10 random spots on the outer regions of the cross-sectional samples is reported in Table VIII along with the error bars (95% confidence level) in the analyses. The totals do not equal 100%, but represent some of the errors in the analyses and the effect of non-ideal specimens. Due to rounding on the edges of the samples and porosity in some of the samples, the totals are low. In particular, 6277 and 7484 had low totals, and these metallizations will be shown to contain more porosity than the other compositions. Note the approximate detection limits for each element.

Table VIII--Compositions (in w/o) of Outermost Region of Metallization

Element	Limit	5081/5082	6160	6175	6277	7484
Ag	0.25	100.60±0.5	98.25±0.55	82.29±1.33	80.70±2.57	67.92±3.27
Al	0.015	0.12±0.01	0.15±0.01	0.35±0.24	0.18±0.08	0.27±0.20
Bi	0.08	0.01±0.01	0.01±0.01	0.30±0.28	1.87±1.38	2.89±2.25
Ca	0.02	-	-	0.02±0.01	0.01±0.01	0.01±0.01
Co	0.06	0.03±0.01	0.02±0.01	0.05±0.02	0.03±0.01	0.29±0.15
Cu	0.1	0.11±0.02	-	0.14±0.13	0.10±0.05	0.16±0.14
Mg	0.02	-	-	0.03±0.03	0.01±0.02	0.04±0.06
Ni	0.07	0.04±0.02	-	0.04±0.02	-	0.03±0.01
Pb	0.09	-	-	0.14±0.14	0.03±0.03	0.29±0.25
Pd	0.05	0.011±0.01	0.02±0.01	16.48±0.27	13.53±0.41	22.10±1.18
Pt	0.1	0.81±0.15	-	0.04±0.02	-	-
Ru	0.1	-	-	-	0.40±0.44	0.72±0.75
Si	0.015	-	-	0.04±0.06	0.08±0.08	0.11±0.14
Zn	0.03	-	-	0.05±0.08	0.02±0.03	-
Total	–	101.72±0.75	98.45±0.59	99.96±2.63	96.96±5.11	94.83±8.41

The major elemental constituents of the metallization layer are representative of the manufacturer's reported weight percentages in the paste, and trace residual elements are either present in the matrix of the metallization or contained within particulate phases within the matrix. The results presented in Table VIII can be simplified to the following approximate matrix compositions for the outer edges of the metallizations (in weight percentage):

5082--99 Ag, 1Pt
6160--100 Ag
6175--83 Ag, 17 Pd
6277--85 Ag, 2.7 Ru, 14.3 Pd
7484--74.7 Ag, 1 Ru, 24.3 Pd

Metallization substrates were examined in plan view and in cross-section. Plan view SEM micrographs are shown in Figure 11, and cross-sectional SEM photo-micrographs are shown in Figure 12. The metallizations exhibited varied grain size, porosity, and surface features including particles in grains and along grain boundaries. The grain size and some of the qualitative chemistry of the particles are reported in Table IX along with the porosity, determined from the cross-sectional microstructures and plan view images.

Table IX--Metallization Microstructural Constituents

Metallization	Grain Size (μm)	Porosity (v/o)	Thickness (μm)	Particle Chemistry
5081/5082	5-15	4.1±1.8	22 total	-Al, Ca, Si, O -Ag, S
6160	10-20	0.6±0.5	10	-Al, Ca, Si, O
6175	1-3	2.8±1.6	8	-Cu, Al, Mg, O -Cu, Zn, Mn, Al, Mg, Si, Bi, O
6277	1-4	10.9±2.1	12	-Bi, Ag, Si, O -Pd, Ru, Bi, Ag, O
7484	1	5.9±1.3	8	-Ca, Ag, Pd, Pb, Al, Si, O -Ca, Bi, Ru, Al, O -Bi, Co, Ag, Pd, Ru, Al, Mg, O

From the cross-sectional images, the thickness of the metallizations, the compositional make-up of the metallization and interaction with the alumina substrate were investigated. The following observations were made:

5081/5082--The double layer metallization in Figure 12a consists of a porous inner layer (about 8% total) and a more compact outer layer. The total thickness of the metallization was about 22 μm. While the inner layer contains silver, platinum, ruthenium, and bismuth, no ruthenium or bismuth is detected in the outer layer. Two oxide phases exist in the interfacial region of the substrate and metallization. One phase, present in smaller quantities, contains magnesium, copper, zinc, silver, manganese silicate. The other phase, a magnesium-rich phase containing copper, silver, zinc, aluminum silicon oxide, is observed along the metallization/substrate interface and might represent the presence of a spinel phase. The enrichment of magnesium at the interface is accompanied by a magnesium-depleted zone of approximately 25 μm in width through the substrate immediately adjacent to the metallization. In addition, this interdiffusion zone contains a copper, bismuth, lead, calcium, cadmium, silver, aluminum silicon oxide phase in the grain boundaries of the alumina substrate. The fine size of the grain boundary glass phase and the interfacial phases as compared to the extended interaction volume of the electron microprobe limited accurate compositional analyses.

6160--The metallized layer contains silver (Figure 12b), and the grain boundary phase in the alumina substrate adjacent the metallization contains a copper, bismuth, silver, calcium silicon oxide compound. No magnesium-depleted zone was detected in this sample.

6175--The metallization in Figure 12c contains at least two phases of which the major phase is a silver and palladium matrix. Another phase possibly containing copper, lead and silver, and zinc from the metallization and magnesium, silicon, and oxygen from the substrate can be observed, especially in the vicinity of the metallization/substrate interface. It was not ascertained as to whether this phase is a spinel phase. Note that adjacent the metallization in the interdiffusion region exists a magnesium depleted zone of about 20 μm in width, also the width of the interdiffusion zone. In the interdiffusion

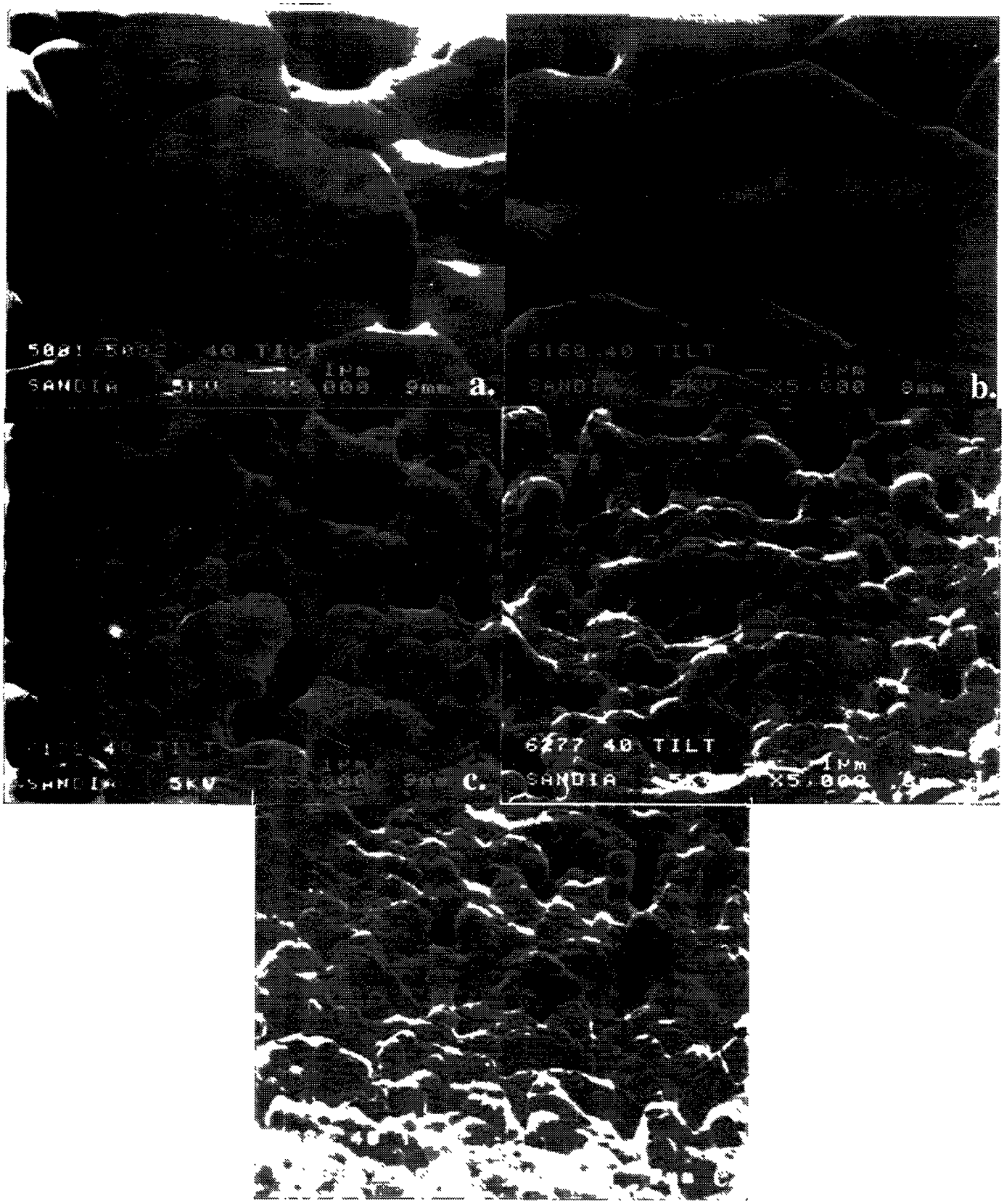

Figure 11--Plan View SEM images of as-fired metallization surfaces. a.) 5081/5082, b.) 6160, c.) 6175, d.) 6277, e.) 7484

Figure 12a--Metallization 5081/5082

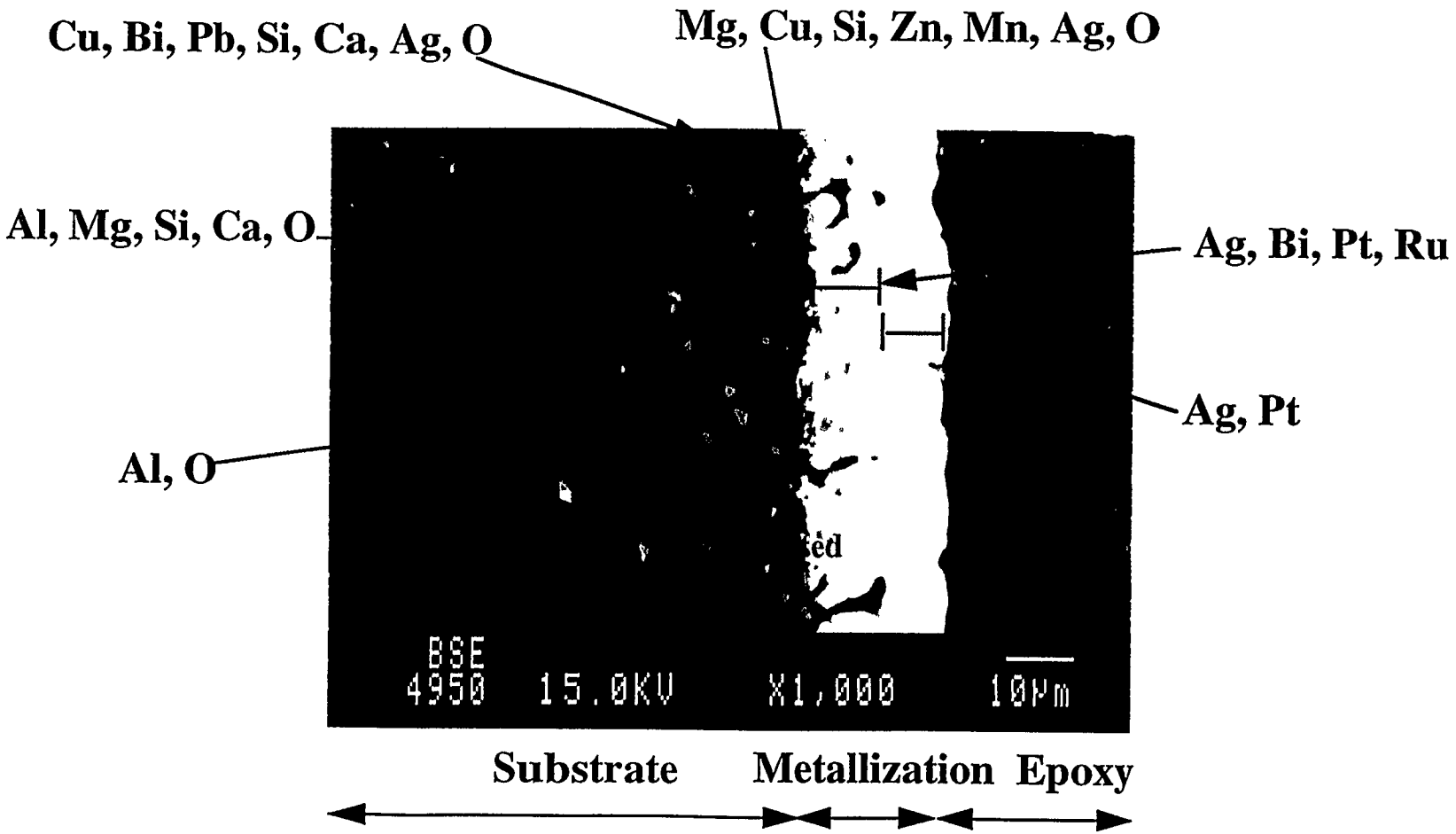

Figure 12b--Metallization 6160

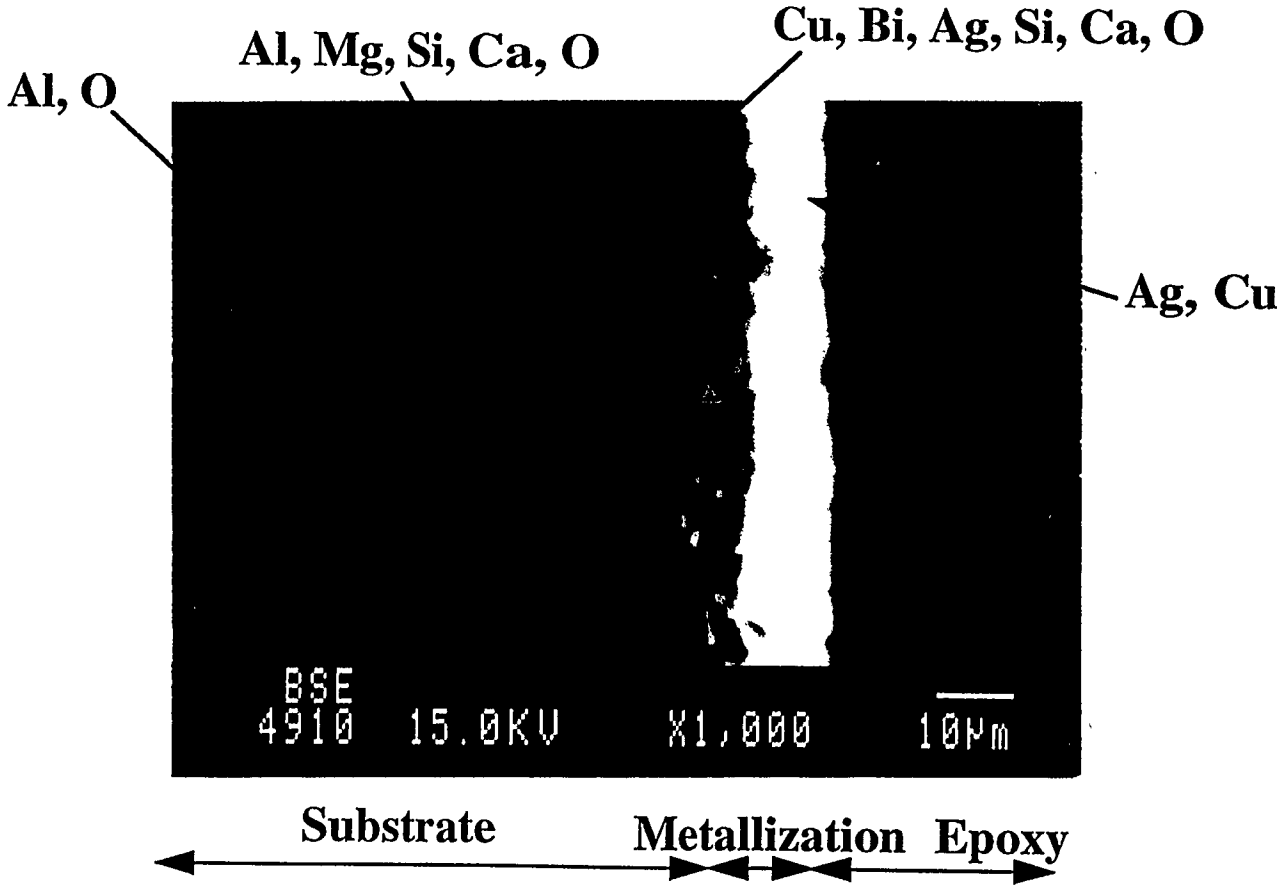

Figure 12c--Metallization 6175

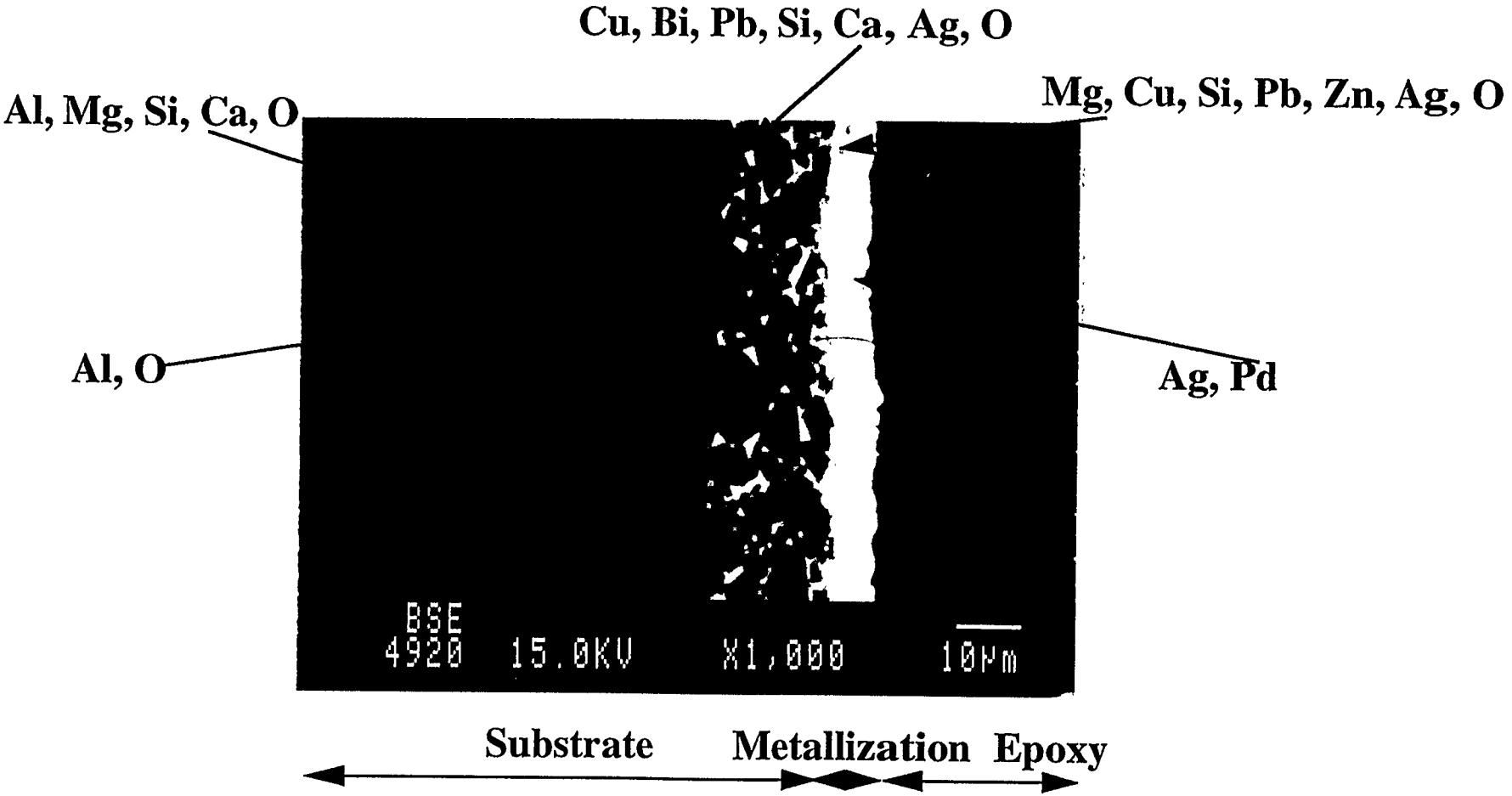

Figure 12d--Metallization 6277

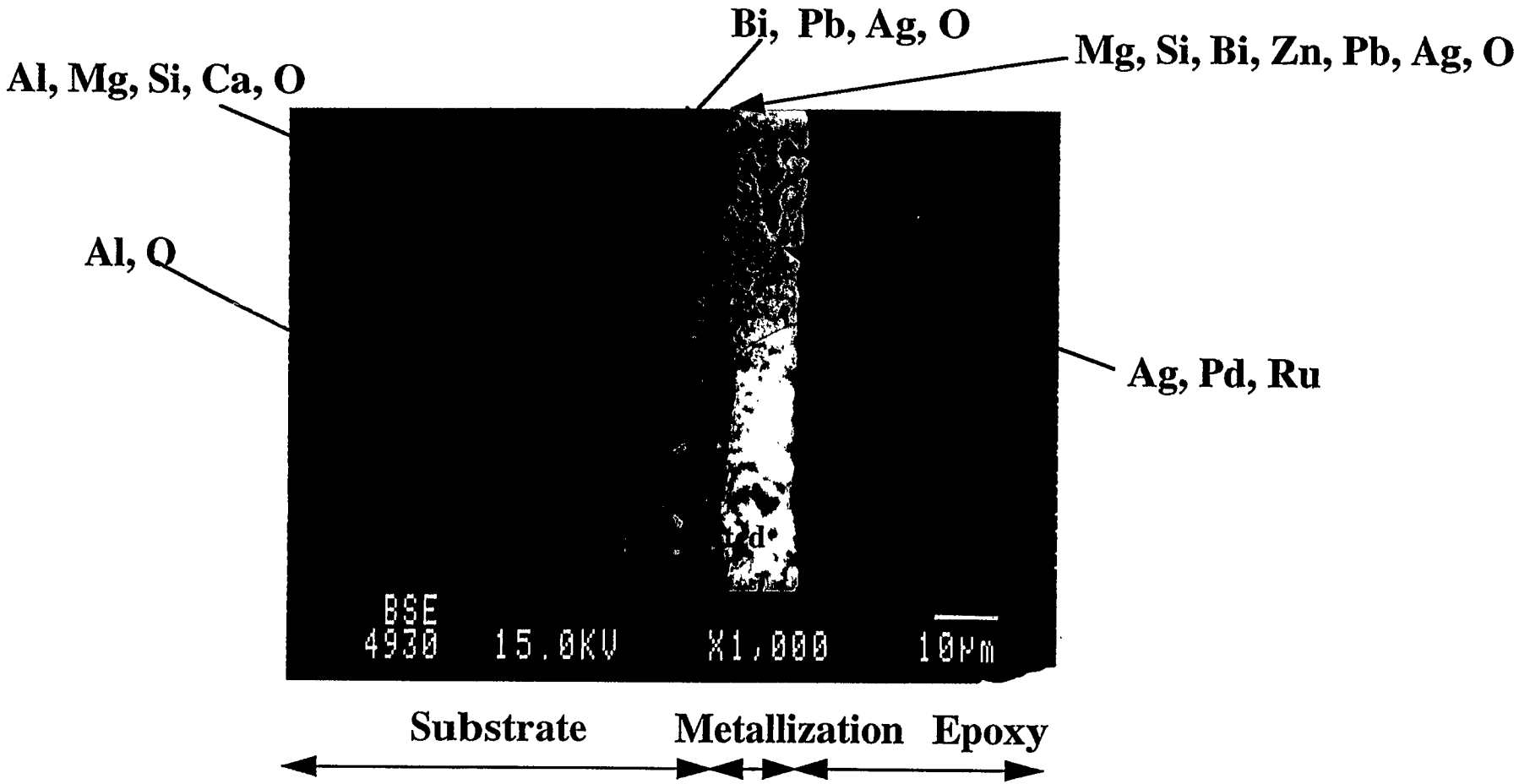

Figure 12e--Metallization 7484

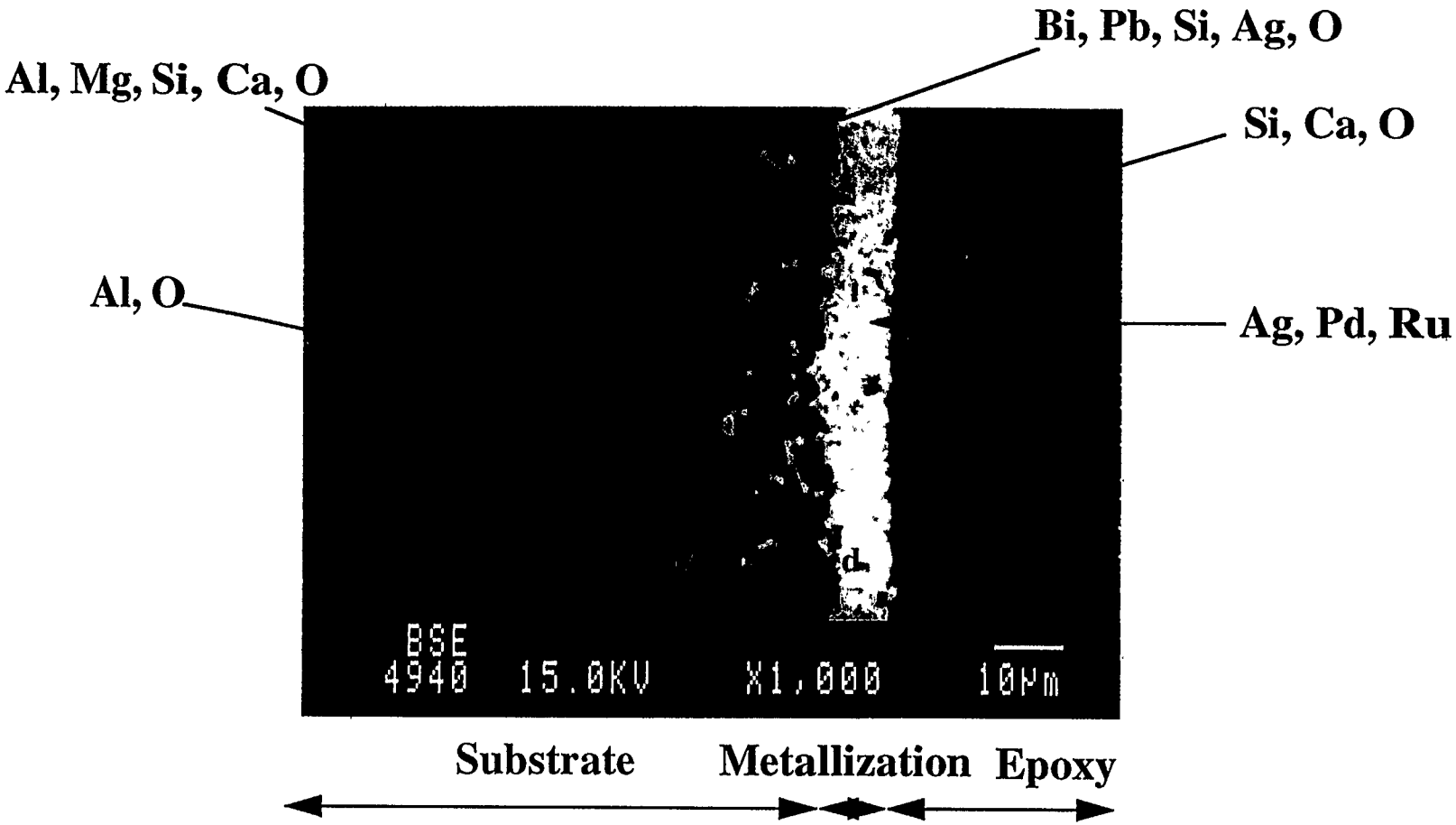

zone a copper, bismuth, lead, calcium, aluminum silicon oxide phase is observed to have formed along the grain boundaries in the alumina substrate.

6277--A similar microstructure is observed for 6277, shown in Figure 12d. The metallization contains silver, palladium, and ruthenium plus a second phase containing ruthenium, bismuth silicon oxide. The metallization/substrate interface contains a zinc, bismuth, magnesium, aluminum silicon oxide. A 15 μm magnesium-depleted zone exists adjacent to the metallization in the substrate throughout which a bismuth, lead, silver oxide resides in the grain boundaries of the alumina substrate. A ruthenium-rich phase is also detected in the metallization. The metallization is porous to about 11%.

7484--The metallization in Figure 12e contains silver, palladium, and ruthenium. Dispersed in the metallized layer is another phase containing calcium silicon oxide, indicating that these elements are diffusing (or flowing by viscous flow) towards the surface of the metal from the substrate. Adjacent to the metallized layer is a 12-15 μm magnesium-depleted zone in the substrate. In this zone resides a bismuth, lead, silver, silicon oxide in the grain boundaries of the alumina substrate. Although a magnesium-depleted zone is observed, no magnesium enrichment is obvious in the metallization/ substrate interface or in the metallization itself. The metallization porosity is about 5%.

Dissolution of the metallization from the substrate allowed the observation of the glass and possible spinel phases that formed along the metallization/substrate interface. Figure 13a shows a finger-like formation that interpenetrated the metallization of 6160. These finger-like formations provide a mechanical interlocking of the metallization with the substrate. Another mechanism that contributes to adherence of the metallization to the substrate is the presence of a spinel (magnesium aluminum oxide) phase or a dense glass/metal structure[16]. Figure 13b shows a fine crystalline phase containing magnesium, bismuth, lead, silver, aluminum silicon oxide at the metallization/substrate interface of 6277. The oxide phases observed in the cross-sectional micrographs of the metallizations provide a method of adhesion of the metallization to the substrate.

Solder/Metallization Microstructures

The metallizations, solders, and fluxes chosen based upon the contact angles and appearance in the first down selection were then processed using the Heller oven. For this effort, the solder materials were in the form of 20 mg solder balls. After processing, samples were mounted in cross-section, polished, and examined in the SEM using back-scattered electron imaging and electron microprobe analysis. Samples formed by hot plate processing were also examined for comparison.

The sessile drops on the 6277 and 7484 metallizations were not well formed, showing examples of dewetting and excess spreading, see Figure 14a. Furthermore, the metallization layers of the 6277 and 7484 samples were highly alloyed with the solder and no recognizable metallization layers remained. These results were the same regardless of the flux and solder types. The alloying of the 6277 metallization with the Indalloy 121 solder (no clean flux) is shown in Figure 14b as a representation of the cross-sections of solder on 6277 and 7484 metallizations.

Sessile drops on 5081/5082 metallization using the no clean flux were all smooth and well-formed to smooth with footing, i.e. Value 1 to Value 2. The representative cross-section of the Sn-Ag-Cu solder and metallization is shown in the backscattered SEM image in Figure 15a. At higher magnification, see Figure 15b, the tortuous interface between the solder and the metallization shows evidence of interaction between the two materials, but the metallization can still be identified. Possibly, the increased thickness of this metallization as compared to the other metallizations has contributed to

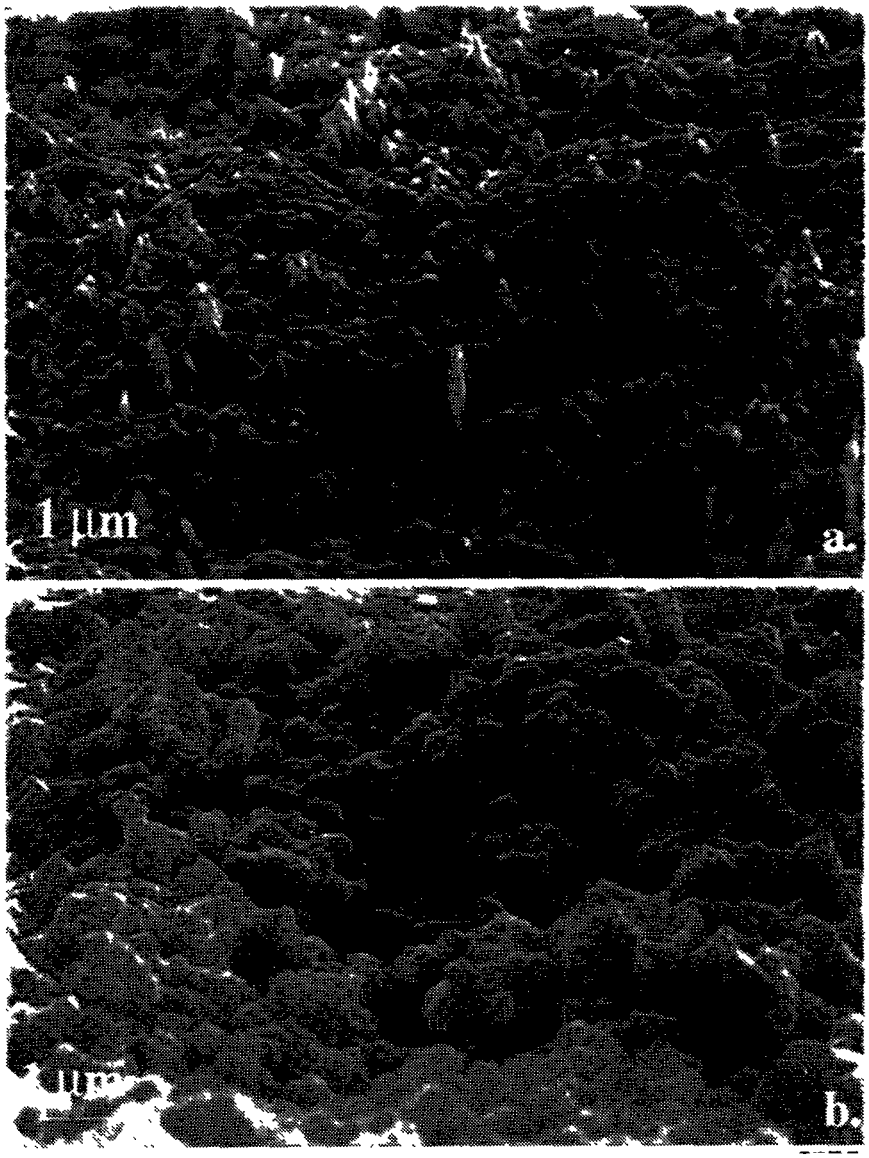

Figure 13--a.) Finger-like formation interpenetrating 6160 metallization from alumina substrate. b.) Finely crystalline phase present between 6277 metallization and alumina substrate.

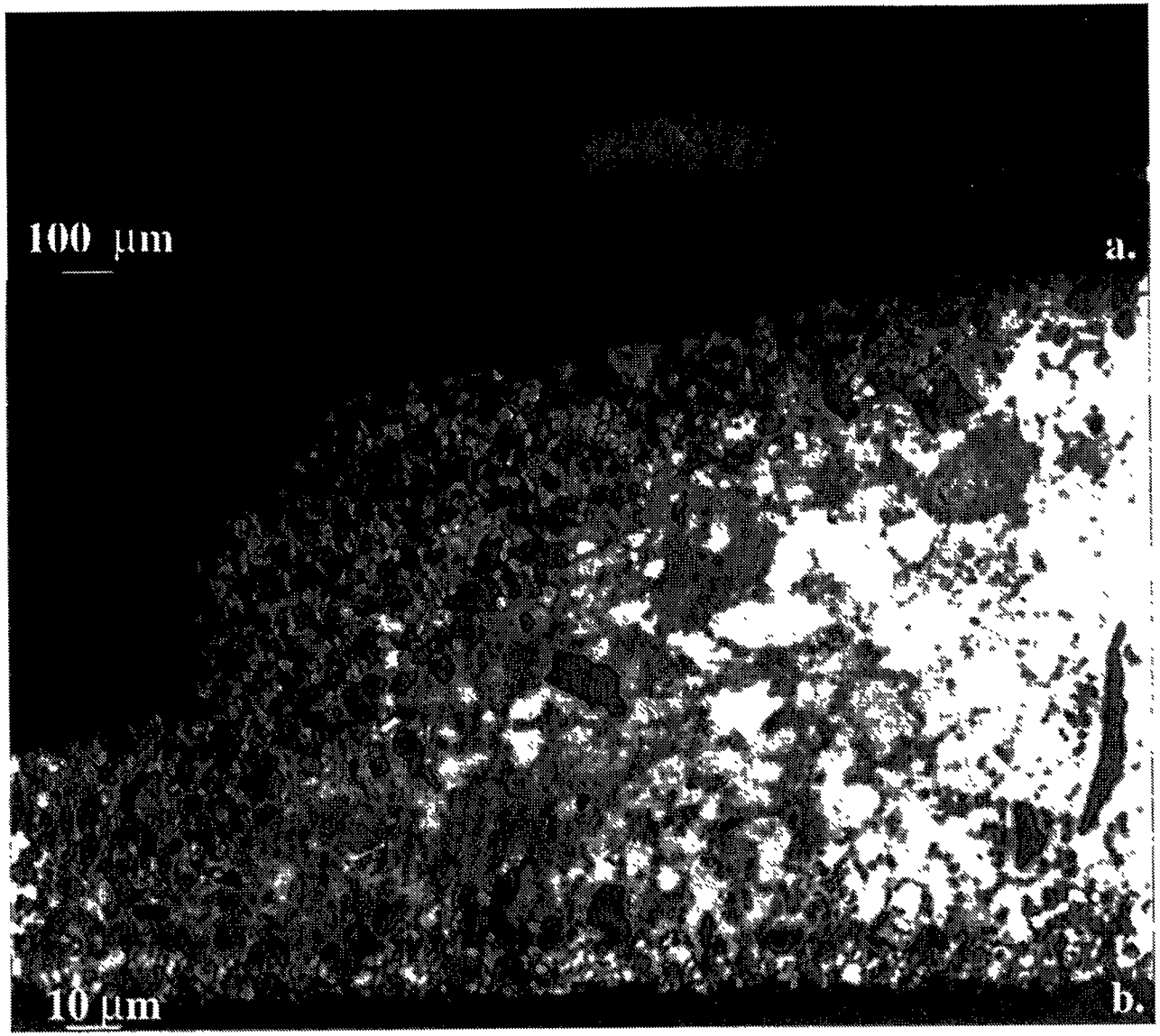

Figure 14 - Cross-sectional images of Indalloy 121 solder on 6277 metallization formed by hot plate processing.

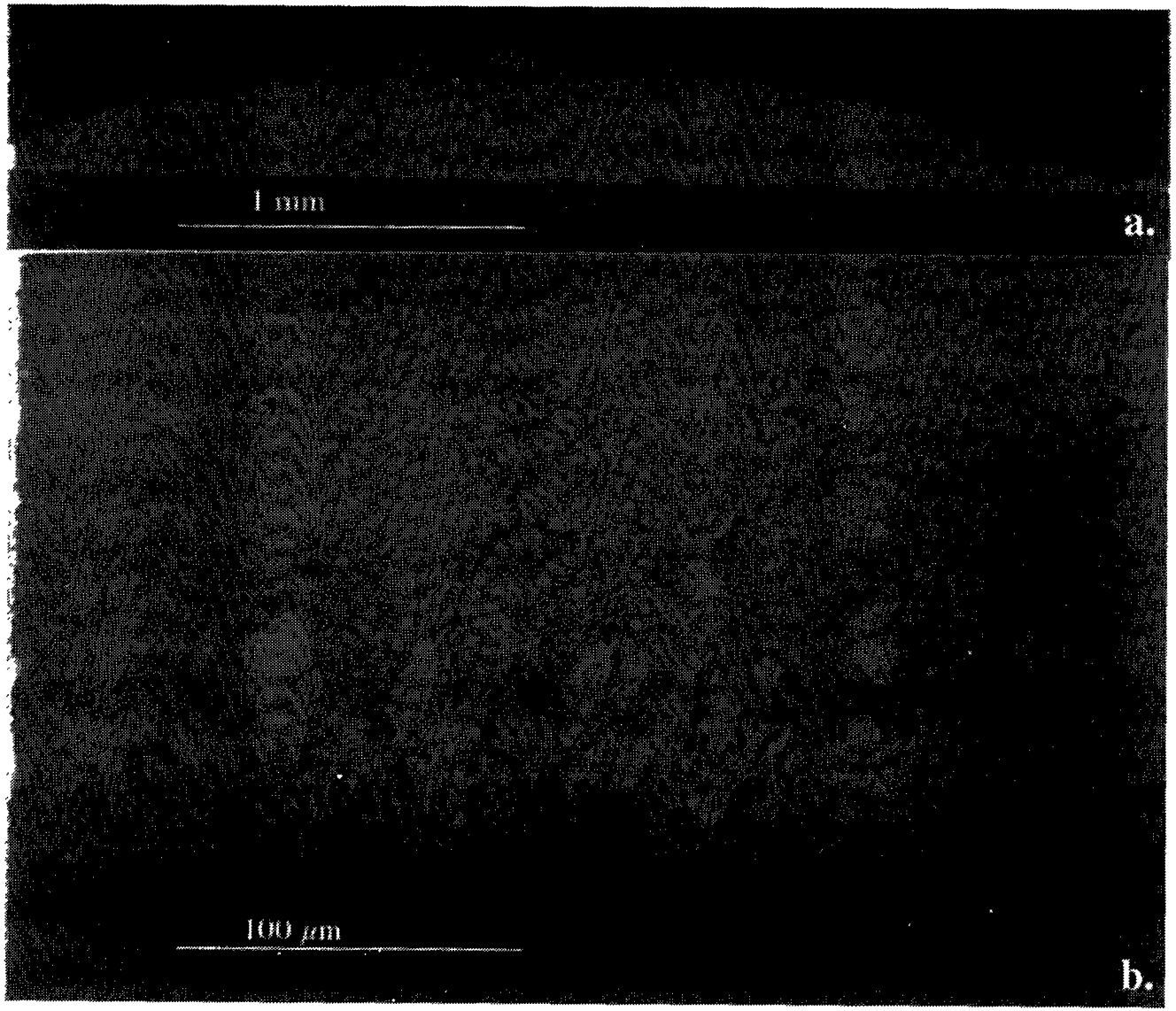

Figure 15 - Cross-sectional images of Sn-Ag-Cu on 5081/5082 metallization formed by hot plate processing.

the greater stability of the metallization during soldering and the lack of dewetting of the sessile drop.

From the appearance of the sessile drop, contact angle, and microstructure, four metallizations (using no clean flux and metallization 5081/5082) would be appropriate for continued investigation--Indalloy 121, Sn-Ag-Bi, Sn-Ag-Cu, and Sn-Cu-Ag-Bi. Figures 16-19 show backscattered SEM images of the cross-sections of the four chosen solders on 5081/5082 metallization for both hot plate and Heller oven processing.

The Indalloy 121 solder heated on the hot plate has a fine eutectic microstructure of Ag_3Sn and Sn containing trace amounts of silver, see Figure 16a. The fine microstructure is a result of the rapid cooling rate that the solder encountered during the thermal processing. Grains of Sn surrounded by rod-like ε-phase Ag_3Sn in the grain boundaries can be observed close to the metallization. Large grains (several microns in width and 10 μm or greater in length) of the intermetallic Ag_3Sn form a continuous layer about 10 μm thick atop of the metallization. The metallization beneath these grains was identified as Ag-0.8w/o Pt. Close observation of the metallization shows that the metallization is no longer continuous over the substrate but regions where the Ag_3Sn contacts the substrate are apparent. The metallization thickness has decreased from over 20 μm to about 10 μm.

By comparison, the Indalloy 121 solder heated in the Heller oven has a coarse microstructure indicative of a slower cooling profile than experienced by the hot plate sample. Large plates of primary Ag_3Sn are present randomly throughout the microstructure, sometimes being viewed on end as long, narrow features and sometimes viewed in the wide dimension (see Figure 16b). These large plates probably formed before the solder solidified so that their orientation is random in the microstructure. The matrix is Sn-rich with traces of silver and regions of fine and coarse eutectic microstructure are observed. A round lead-containing particle (not shown in the image) was found in this microstructure, presumably due to lead from the oxide phases present at the original metallization/substrate interface or from the glass phase in the alumina. The original metallization is not continuous along the substrate, and the Ag_3Sn layer atop the metallization penetrates to the substrate.

One feature observed in the Indalloy 121 solder heated in the Heller oven contained platinum and tin with trace amounts of silver. Compositional analysis utilizing the electron microprobe indicated that the phase had a stoichiometry of $PtSn_7$ with <0.5 w/o Ag substituted on platinum sites. No such phase has been identified in the binary equilibrium platinum-tin phase diagram[17]; the possibility that this is a non-equilibrium phase exists. Other platinum-tin features in the form of rods were detected in the microstructure of both the Indalloy 121 hot plate and Heller heat treated materials. Due to their fine size, the exact composition of the rods were not determined, however it is believed that their composition is closer to $PtSn_4$, an equilibrium phase in the Pt-Sn binary system. These features can be seen as thin white needles or rods (see arrows in Figure 16a and b) between the eutectic colonies in the microstructure. The distance of these rods from the metallization indicates that platinum was rejected into the liquid solder during the formation of Ag_3Sn from the contact of the solder with the metallization.

The microstructure of the eutectic Sn-Ag-Cu solder heated on the hot plate is shown in Figure 17a. A microstructure very similar in appearance to the Indalloy 121 solder heated on the hot plate is seen, however no platinum-tin phase was observed. The microstructure varies in that the structure is finer, and copper is present in both the Sn-rich regions (trace constituent) and in the eutectic regions. The exact composition of the eutectic features was not determined due to their fine size. In the ternary eutectic, nearly pure Sn, Ag_3Sn, and Cu_6Sn_5 should be present. It was observed that copper enrichment existed between the eutectic colonies, suggesting that a divorced eutectic may be present.

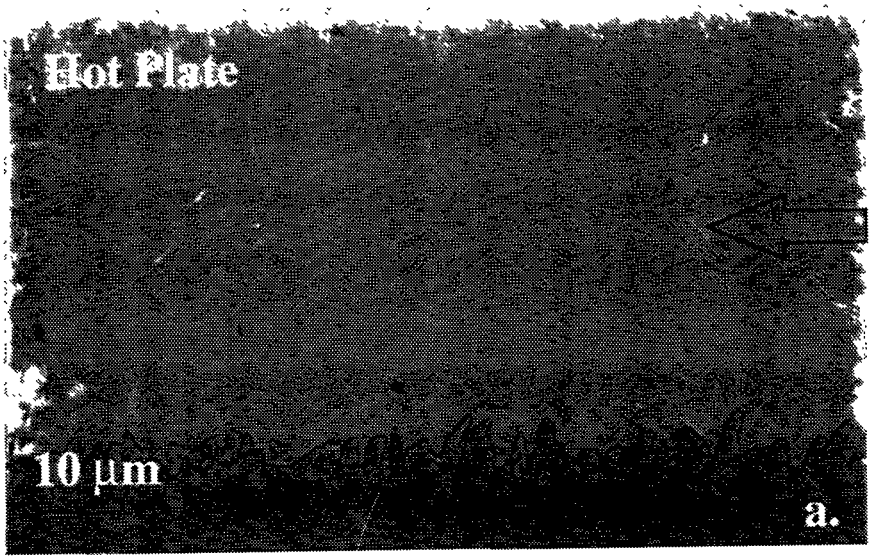

Figure 16 - Indalloy 121 solder on 5081/5082 metallization.

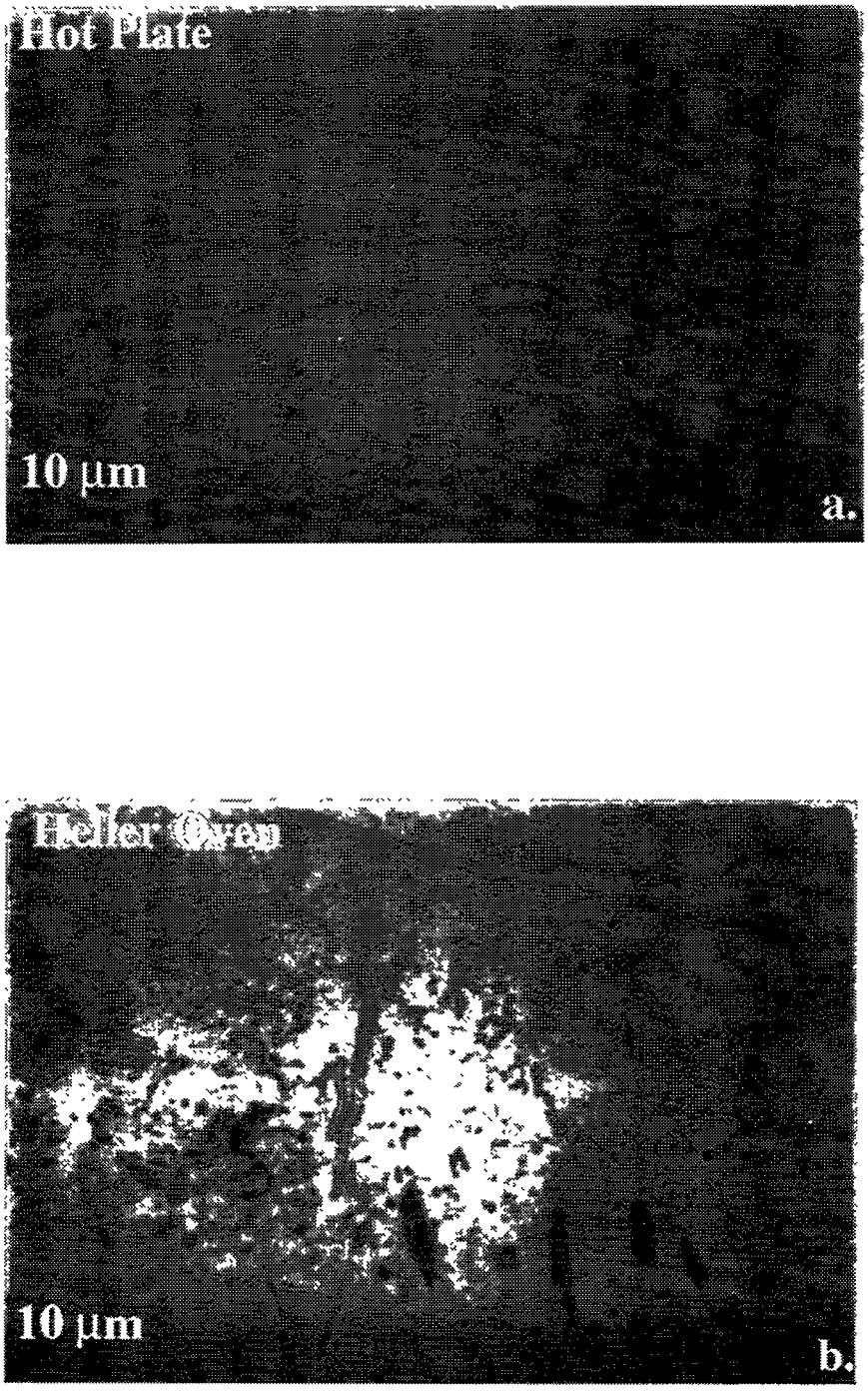

Figure 17 - Sn-Ag-Cu solder on 5081/5082 metallization.

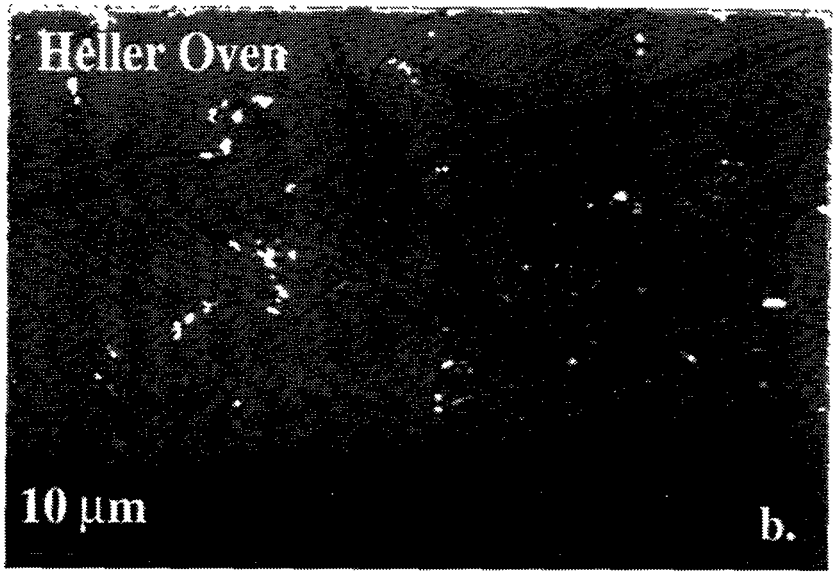

Figure 18 - Sn-Ag-Bi solder on 5081/5082 metallization.

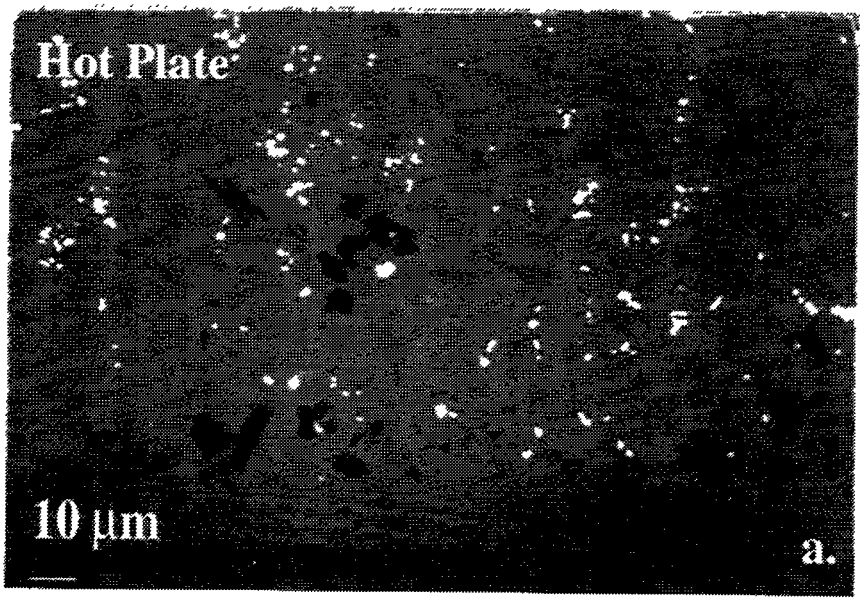

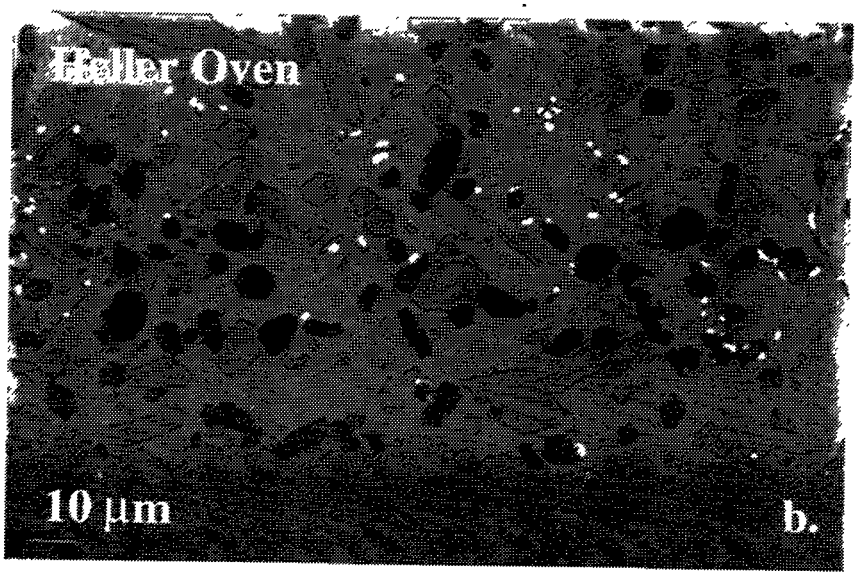

Figure 19 - Sn-Ag-Cu-Bi solder on 5081/5082 metallization.

Divorced eutectics may be produced under conditions of large undercoolings [18]. A layer of large Ag_3Sn grains cover the remaining metallization, whose composition was determined to be Ag-0.8 w/o Pt.

The microstructure of the Sn-Ag-Cu solder heated in the Heller oven is shown in Figure 17b. Again, a coarser microstructure is observed due to the slower cooling rate of the Heller oven. The microstructure contains large primary Ag_3Sn, coarse eutectic Sn, Ag_3Sn, and Cu_6Sn_5, and large primary Cu_6Sn_5 with 0.9 w/o Pt and 0.6 w/o Ag substituted for the Cu in this phase. The Ag-1 w/o Pt metallization has decreased in thickness to about 10 μm, and a layer of large grains of Ag_3Sn is present atop the metallization.

The Sn-Ag-Bi solder on the 5081/5082 metallization contains a Bi-rich phase that should be essentially pure Bi, apparent in the microstructure as small round white regions (see Figure 18 a and b). The microstructure of the sample formed on the hot plate (Figure 18a) contains the Sn-Ag eutectic whose colonies are surrounded by primary Sn and the Bi phase. Close to the metallization region much Sn exists and large grains of Ag_3Sn form a continuous layer over the Ag-0.5 w/o Pt metallization. The microstructure of the Sn-Ag-Bi solder formed in the Heller oven is again coarse by comparison to its hot plate counterpart. Large primary Ag_3Sn plates are randomly oriented through the microstructure and small round Bi particles are present. The metallization region is the same as in the hot plate microstructure.

In Figure 19 a and b, the microstructure of the Sn-Cu-Ag-Bi solder on 5081/5082 metallization is shown for both hot plate and Heller oven thermal processing. The sample formed on the hot plate has a eutectic microstructure with round white Bi particles, a Sn-rich matrix and Cu_6Sn_5 between the colonies. Closer to the metallization, regions of the Sn-rich matrix containing some Bi are seen to be separated by eutectic or Ag_3Sn regions. Large primary Cu_6Sn_5 grains appear as equiaxed and plate-like dark regions in the microstructure; silver in 0.4 w/o is measured in the large equiaxed grains. Below the Sn-rich region is the layer of large Ag_3Sn grains atop the remaining Ag-Pt metallization. In the microstructure of the sample formed in the Heller oven, a coarse overaged microstructure with large grains of Ag_3Sn and Cu_6Sn_5 containing minor amounts of Pt and Ag and small round grains of Bi are observed in the Sn-rich matrix. An alloyed layer of Ag_3Sn exists above the metallization of Ag-0.65 w/o Pt that has changed little from its original thickness. In Figure 20, a low magnification image of this sample shows the non-uniformity of the sessile drop microstructure in which the copper-rich phase is distributed mostly through one half of the solder and not the other. An inhomogeneous starting material may contribute to the sessile drop inhomogeneity; this is being investigated.

Down Selection Procedure

The initial matrix of 120 combinations of 6 alloys, 5 metallizations, and 4 fluxes was wetted on the hot plate with only a single replicate of each. The second set of experiments had 24 trials (4 alloys, 3 metallizations, and 2 fluxes); this set was processed in the Heller oven, and had two replicates each. Multiple replications were performed on the down selected trials to improve the statistics. This was made possible by the smaller number of trials (24 vs 120). These results were compared to the hot plate data. This led to the selection of 4 trials (4 alloys, 1 metallization, and 1 flux) to remain for further testing. This down selection procedure was based on analysis of the contact angles, appearance of the sessile drops, and microstructural and corrosion data on the metallization. Figure 21 shows a flow chart representing the down selecting process.

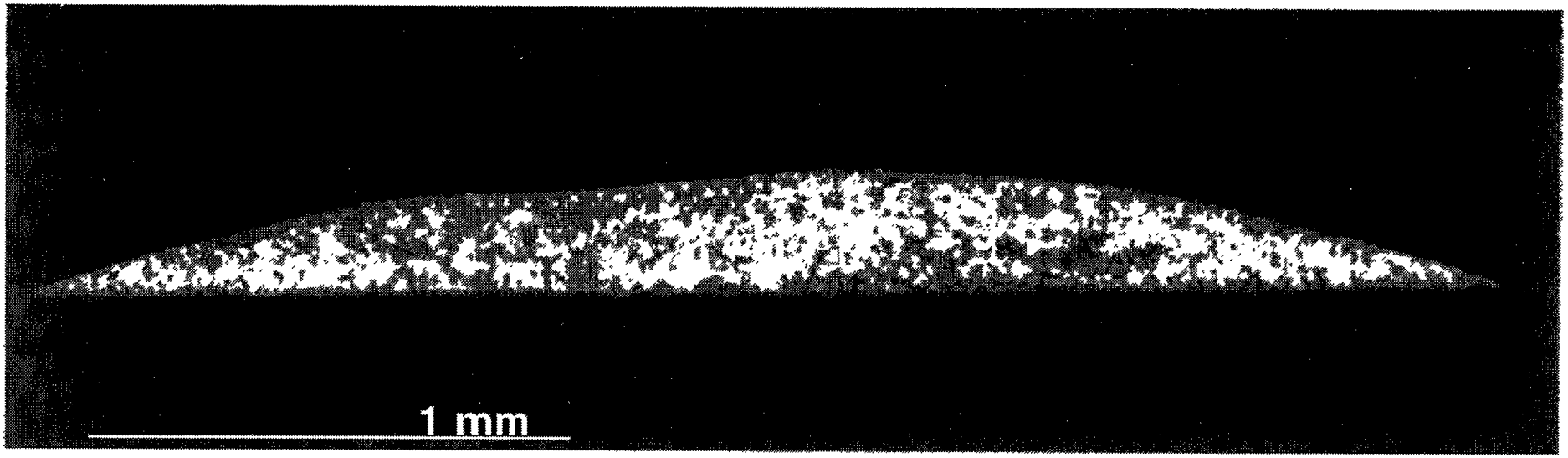

Figure 20 - Low magnification of Sn-Ag-Cu-Bi solder on 5081/5082 metallization showing non-uniformity of solder microstructure.

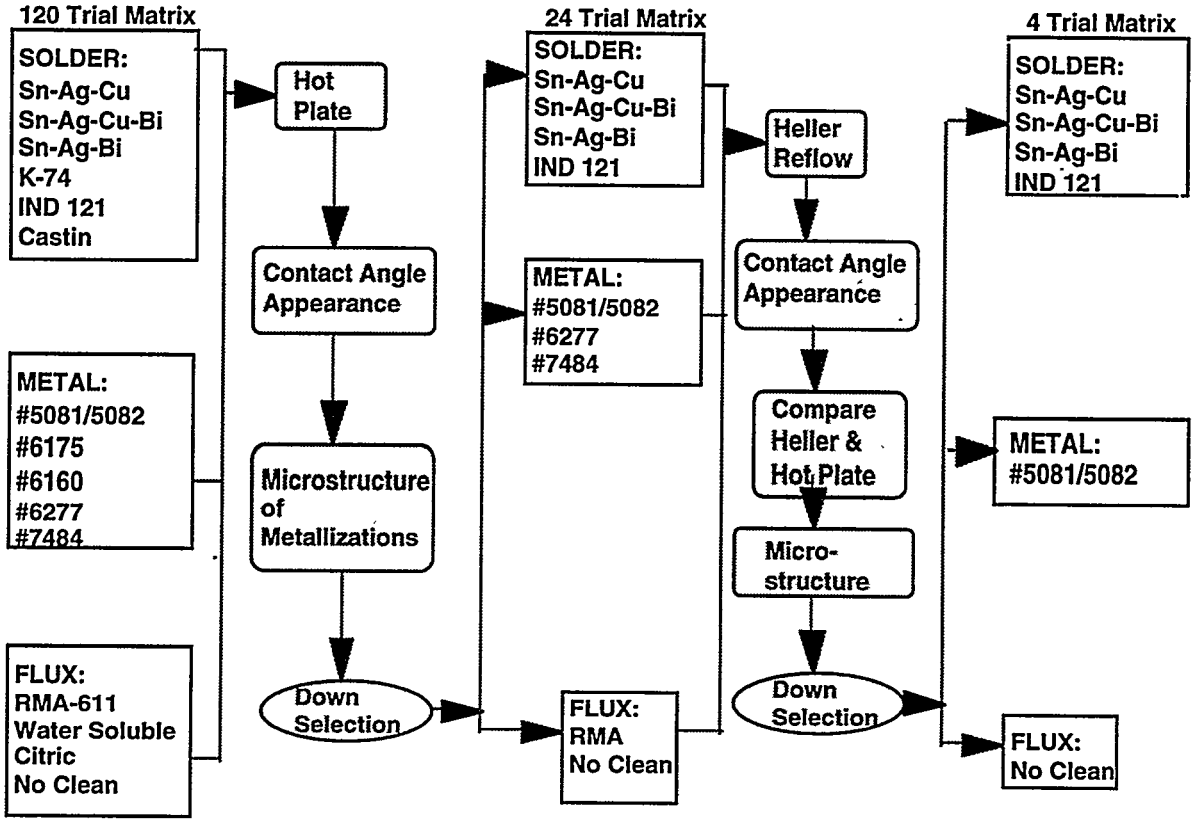

Figure 21--Flow chart showing the down selecting procedure.

DISCUSSION

Plotting of the appearance, contact angle, and product of the appearance and contact angle for each of the main factors--six solder alloys, five metallizations, and four fluxes--allowed for the selection of 5081/5082 as a metallization that could provide low contact angles, good appearances, and therefore a low product of appearance and contact angle. The high amount of variability in the other data and the high levels of significance of each factor upon the contact angles and appearances made down selection difficult without the use of other information. An initial down selection was made from 120 combinations to 24 combinations. The final down selection to 4 combinations based upon microstructural analysis is only tentative as explained below.

For the processing times and temperatures used in this experiment, the Ru-Pd containing metallizations fully alloyed with the solder. Thicker substrates should be investigated in order to determine if a more rapid alloying reaction is in fact occurring in these materials during soldering as compared to the Ag-Pt metallization 5081/5082 or if the thickness of the 6277 and 7484 metallizations was simply insufficient so that complete alloying of the solder with the metallization occurred. The thickness to which the 5081/5082 metallization alloyed with the metallization was on the order of 10 μm, which is approximately equal to thicknesses of all of the other metallizations.

In addition to this recommendation, some other recommendations are provided. The aging of metallization solder samples of the chosen materials--Indalloy 121, Sn-Ag-Bi, Sn-Ag-Cu, and Sn-Ag-Bi-Cu based solders as described herein--can be predicted by the appearance of the Heller oven processed samples. Coarsening of all phase components should be expected, and continued alloying of the metallization with the solder to form Ag_3Sn will occur. The layering of phases in the microstructure adjacent the substrate cannot fully be predicted at this point. However, from the presently observed microstructures, it is apparent that an intermetallic is forming in the interface of the solder and the metallization. This layered intermetallic may lead to undesirable mechanical properties; therefore, the strength of the solder-metallization bond should be investigated before and/or during aging studies.

The microstructures obtained from the rapid cooling rate employed during hot plate processing is a more desirable microstructure from a mechanical properties point of view. That is, the fine features of the eutectic microstructure should impart greater mechanical strength to the solder joint. The coarser structures obtained by Heller oven processing are undesirable in that the large intermetallics are brittle and may fracture under stress. Modifications to the cooling cycle of the Heller oven processing are highly recommended before aging studies begin.

The eutectic Sn-Ag system consists of two phases--Sn-rich matrix containing <0.04 w/o Ag in solution and the ε-phase intermetallic. Yang and others[19] report that the rod-like structure of the Ag-Sn intermetallics tends to minimize the surface energy associated with the phase interfaces, thus their presence as rod-like structures throughout the Sn matrix is expected. Their size and morphology is however a function of the cooling rate during solidification. Aging of the Sn-Ag system results in coarsening of the ε-phase. A growth rate of an Ag_3Sn intermetallic layer in an Ag-Sn couple at 190°C was determined[19] to be 4.43×10^{-9} m/s$^{1/2}$. Due to the layering of this intermetallic in the microstructure, initial mechanical tests should be performed before aging studies begin.

The formation of Cu_6Sn_5 intermetallics during the solder ing of eutectic Sn-Ag on copper has been reported in the literature[19]. Copper is dissolved into the solder during soldering, forming Cu-Sn intermetallics in the bulk solder or layers of Cu-Sn intermetallics at the solder-copper interfaces. With copper present in the solder alloy, the formation of Cu-Sn intermetallics occurred in this study, and evidence of their coarsening with slower cooling rates in the Heller oven suggests that coarsening will also occur during aging of the solder alloys. Two intermetallics form in the Ag-Sn solders--the η-phase Cu_6Sn_5 as reported herein and the ε-phase Cu_3Sn which was not detected in this preliminary investigation of these solders. The formation of these brittle intermetallics at the solder-copper may need to be investigated for their influence upon mechanical integrity of the joint if copper leads are to be used.

At present, four solders are being considered for use on 5081/5082 metallization using a no clean flux. The preliminary results indicating promising properties from four solders hints at the possibility of a robust system for solder alternatives in high temperature, underhood applications. Thicker metallizations of 6277 and 7484 may show that promising results can be obtained with these metallizations as well. However, continuing down selection will occur as aging studies and other preliminary mechanical properties are established.

CONCLUSIONS

1. For high temperature, underhood applications, six Pb-free solders, four fluxes, and five silver-based metallizations were investigated for wetting behavior, sessile drop appearance, and microstructure. Solder systems were initially screened using low contact angles and desirable sessile drop appearances as the evaluation criteria. Finally, solder systems were screened based upon microstructural observations.

2. The following down selections were made:

   i.) Low contact angles and desirable sessile drop appearances were obtained for the Sn-Ag-Bi, Sn-Ag-Cu, Sn-Ag-Cu-Bi, and Indalloy 121 on metallization 5081/5082 using no clean flux. These combinations have been chosen for subsequent testing.
   ii.) The pure silver metallization 6160 was not selected due to apparent corrosion problems.
   iii.) Ruthenium and palladium containing metallizations were not selected due to poor sessile drop appearances, however they will be reinvestigated for sessile drop appearance and contact angle using thicker metallization.
   iv.) The citric and water-soluble fluxes were not selected due to high contact angles and appearance values. The citric acid flux also caused discoloration of the metallization on samples formed in air. Ultimately, the no clean flux was selected because no difference in response was observed between RMA and no clean when heating in an inert atmosphere, and no clean is the desired industrial flux.
   v.) The Castin and Sn-Ag-Bi-Sb solders were not selected due to high contact angles and appearances and to brittle intermetallic formation, respectively. The other four solder alloys are still under consideration.

3. For ruthenium and palladium containing metallizations the following observations were made:

   i.) surface microstructure contained many particles of varied composition.
   ii.) the grain size of the microstructure was generally finer than other metallizations.
   iii.) the metallizations underwent rapid dissolution and/or intermetallic formation during soldering. More work must be performed to determine whether a thicker metallization will produce desirable microstructures and properties.
   iv.) sessile drop appearances were generally poor. Again, the full alloying of the thin metallization may have contributed to the appearance of the sessile drops, and more work must be performed to determine sessile drop appearance on thicker metallizations.

4. Microstructural comparisons between Heller oven and hot plate heat treatments illustrated larger microstructural constituents existed in the microstructures of the Heller oven samples. This indicated that the Heller heat treatment subjected the material to a slower cooling rate. The coarse microstructures obtained from this processing are undesirable, therefore faster cooling schedules and varied Heller oven profiles will be tried to refine the solder microstructure.

5. For the heat treatments used, layered formation of the intermetallic Ag_3Sn is evident atop the 5081/5082 metallization after soldering. The intermetallic grows by reaction of the Sn-rich solder with the silver metallization. Some

instances of platinum rejection into the liquid solder are evident indicating that rapid intermetallic formation occurs while the solder is still molten. Sn-rich or Ag-depleted regions are visible adjacent the Ag_3Sn intermetallic layer atop the metallizations in the back-scattered SEM micrographs. The mechanical integrity of the initial microstructure will be investigated in light of the layered intermetallic present.

ACKNOWLEDGMENTS

The authors would like to thank the following people for their contributions to this study: F. Uribe, G. Zender, P. Hlava, R. Grant, D. Goel, F. Jeantette, F. Greulich, A. Kilgo, J. Roberts, and A. C. Carter.

REFERENCES

1. Frear, D., Morgan, H., Burchett, S., and Lau, J.: The Mechanics of Solder Alloy Interconnects, Van Nostrand Reinhold, New York (1994)

2. London, J. and Ashall, D. W.: "Made with a Tin/Silver Eutectic Alloy", **Brazing and Soldering**, No. 10 (Spring 198x) p. 17

3. Hwang, J. S. and Vargas, R. M.: **Soldering and Surface Mount Technology**, No. 5 (June 1990), p. 38

4. Soloman, H. D.: "Low Cycle Fatigue of Sn96 Solder with Reference to Eutectic Solder and a High Pb Solder", **Trans. ASME**, Vol. 113 (June 1991) p. 102

5. Davies, R. L.: "High Strength, Low Temperature Bonding with Silver-Tin Solders", **Welding J.**, (October 1976) p. 838

6. Gram, N.: Tin and Its Uses, No. 120 (1979) p. 1

7. Yost, F. G., Hosking, F. M., and Frear, D. G.: The Mechanics of Solder Wetting & Spreading, Van Nostrand Reinhold, New York (1993)

8. Loomans, M. E, Vaynman, S., Ghosh, G., and Fine, M. E.: "Investigation of Multi-Component Lead-Free Solders", **J. Electr. Mater.**, Vol. 23, No. 8 (1994) p. 741

9. McCormack, M. and Jin, S.: "Progress in the Design of New Lead-Free Solder Alloys", **J. Metals** (July 1993) p. 36

10. Miller, C. M., Anderson, I. E., and Smith, J. F.: "A Viable Tin-Lead Solder Substitute: Sn-Ag-Cu", **J. Electr. Mater.**, Vol. 23, No. 7 (1994) p. 595

11. Glazer, J.: "Microstructure and Mechanical Properties of Pb-Free Solder Alloys for Low-Cost Electronic Assembly: A Review", **J. Electr. Mater.**, Vol. 23, No. 8 (1994) p. 693

12. S. J. Sackinger, M. M. Karnowsky, and F. G. Yost, "Development and Characterization of Alloys and Powder Processing Techniques for Lead-Free Solder Pastes", SANDIA Report Sand94-0008/UC-402 (April 1994).

13. Image-Pro Plus software

14. Montgomery, D.C.: Design and Analysis of Experiments: Third Edition, John Wiley & Sons, New York (1991)

15. Solder Mechanics, A State of the Art Assessment, ed. by Frear, D.R., Jones, W.B., and Kinsman, K.R., The Minerals, Metals, & Materials Society, Pittsburgh, PA (1990)

16. Twentyman, M. E.: "High-Temperature Metallizing", **J. Mater. Sci.**, Vol. 10 (1975) p. 765

17. Alloy Phase Diagrams, ASM Handbook, ASM International, Materials Park OH, Vol. 3 (1992)

18. Gordon, P.: Principles of Phase Diagrams in Materials Systems, McGraw-Hill Book Co., San Francisco (1968) p. 158

19. Yang, W., Messler, R. W. Jr., and Felton, L. E.: "Microstructure Evolution of Eutectic Sn-Ag Solder Joints", **J. Electr. Mater.**, Vol. 23, No. 8 (1994) p. 765

DISTRIBUTION

External Distribution:

10 Prof. Marty W. Weiser
Department of Mechanical Engineering
University of New Mexico
Albuquerque, NM 87131

1 Lary R. Hocken
AC Delco Systems
Control Systems Engineering
Department 32-18
1300 North Dort Highway
Flint, MI 48556

1 Larry Hazelton
AC Delco Systems
Control Systems Engineering
Department 32-18
1300 North Dort Highway
Flint, MI 48556

Internal Distribution:

1	MS 0161	M. Moss, 11510
1	MS 0337	A.D. Romig, 1800
1	MS 0339	J.L. Jellison, 1803
1	MS 0340	M.J. Cieslak, 1831
1	MS 0340	M. Essien, 1831
1	MS 0340	C.L. Hernandez, 1831
1	MS 0340	E.A. Holm, 1831
1	MS 0340	F.M. Hosking, 1831
1	MS 0340	D.O. MacCallum, 1831
1	MS 0340	J.A. Rejent, 1831
10	MS 0340	S.J. Sackinger, 1831
1	MS 0340	P.T. Vianco, 1831
15	MS 0340	F.G. Yost, 1831
1	MS 0340	W.R. Cieslak, 1832
1	MS 0340	D.R. Frear, 1832
1	MS 0340	N.R. Sorenson, 1832
15	MS 0342	C.A. Drewien, 1822
1	MS 0367	D.E. Peebles, 1812
1	MS 0368	H.C. Peebles, 1815
1	MS 0609	J.O. Stevenson, 1841
1	MS 0619	Technical Publications, 7151
5	MS 0899	Technical Library, 7141
5	MS 0957	F. Uribe, 2411
1	MS 0957	S. Garrett, 2411
1	MS 1071	T. J. Allard, 2205
1	MS 1073	T. Mirabal, 2272
10	MS 1119	Document Processing, 7613-2
1	MS 9018	Central Technical Files, 8523-2

For DOE/OSTI